Review Article

A review on effect of various artificial roughness on heat transfer enhancement in a channel flow

Sudharani PANDA[1,*] **Rakesh KUMAR**[1]

¹Department of Mechanical Engineering, IIT(ISM) Dhanbad, Dhanbad, India

ARTICLE INFO

ABSTRACT

Heat transfer improvement plays a vital role in several industrial applications as well as in the transportation sector such as gas turbines, heat exchangers, various cooling devices, and combustor liners. The extensive research to enhance the heat transfer rate in various sectors has been carried out to achieve the objectives such as (i) to increase the system efficiency, (ii) to reduce thermal load, (ii) to reduce consumption of non-renewable energy, (iii) to reduce the production of emission, (iv) to develop new green technologies, (v) to lower energy prices for the consumer. The heat transfer in various sectors has been carried out by adopting three different ways (i) increasing the surface area of the heat transfer systems, (ii) enhancing the fluid properties, (iii) by adding extra surface on the heat transferring surface. This article aims to deliver a comprehensive review of the current research on heat transfer enhancement techniques by using artificial roughness elements such as rib tarbulator, fin, and dimple. It includes various types of rib tarbulators, fins, and dimples used for heat transfer enhancement of gas turbine blades of the power plant, combustion liners as well as solar air heaters. The physical mechanism responsible for heat transfer enhancement in various artificial roughness elements has been discussed and compared. The challenges and difficulties associated with the heat transfer techniques have been discussed. The parameters such as dimple depth, channel height to dimple imprint diameter, pitch, the density of artificial roughness element, arrangement of artificial roughness, relative roughness pitch, relative roughness height, angle of attack on flow, mass flow rate, Reynolds number on thermal performance, thermohydraulic performance, flow structure, friction characteristics have been studied and compared. From the comprehensive review, it may be recommended that the teardrop shape dimple can be used for further enhancement of heat transfer as compared to other artificial roughness elements. In the future, this teardrop may be used to enhance the heat transfer in the solar thermal system and some other relevant thermal systems.

Cite this article as: Panda S, Kumar R. A review on effect of various artificial roughness on heat transfer enhancement in a channel flow. J Ther Eng 2021;7(5):1267–1301.

***Corresponding author.**
*E-mail address: sanjimuni@gmail.com

INTRODUCTION

The heat transfer enhancement has been considered to be one of the most promising problems in modern power plant engineering, microelectronic cooling, heat exchangers (macro and micro-scale), cooling of the internal airfoil of a gas turbine, fuel elements of nuclear power plants, solar air heater and even bio-medical devices. The urgency to enhance heat transfer rate dictated due to the following reasons [1],

a) To increase the thermal efficiency of the thermal power plant,
b) To reduce friction factor,
c) To maintain the compactness of heat transfer equipment,
d) To reduce the thermal stress developed in the element of steam power plant engineering and fuel element of nuclear power plants,
e) In order to reduce metallurgical failure and to maintain structural integrity,
f) To increase the life of the components, etc.

So, to full fill all these criteria, many cooling methods have been developed. One cooling approach, which is incorporated with the turbine components such as turbine blade or vane and combustor liner is introduced to the internal cooling passages. Rib roughness or rib turbulators are protruded to enhance the heat transfer rate in the internal cooling passages. Another method that is introduced to improve the rate of heat transfer is the use of pin fins or pin banks. The pin fins are attached to the trailing section of the vanes to enhance the heat transfer rate. However, the uses of protruding element on the surface have some drawbacks as follows [2],

- The ribs protruded from the heat transfer surface induces excessive pressure loss (The friction between the flowing fluid and the surface increases; hence the pressure loss increases).
- The working fluid supply to the inlet of the turbine at a particular pressure or higher pressure but due to the introduction of protruding element on heat transfer surface the pressure loss occurs hence to compensate for this pressure loss the working fluid needs to compress in the compressor at a pressure higher than the desired pressure at the turbine inlet.
- Due to pressure loss, the flow separation occurs on discretely mounted ribs or pin fins; hence there will be non-uniform cooling over the heat transfer surface, and thermal stress developed.
- The advanced internal cooling design with broken ribs of intricate patterns may be difficult to design.
- The excessive rib material added to the system may be undesirable when reducing engine weight to thrust ratio is critical.

The potential of using concavities for heat transfer enhancement has been discussed in many undocumented reports and by Schukin et al. [3]. The idea is to implement the concavities for heat transfer enhancement is a tornado-like a process which bursts from the concavities wall and advances to the flow housed in a channel. The tornado-like jet inherits self-organising vortex motions and promotes turbulent mixing [2]. In other words, the concavities act as vortex generators. A review of the limited data in the Russian report revealed that concavities' use enhanced the rate of heat transfer by 2 to 3 times than the smoother counterpart. However, the gradually outlined concavities enhance the heat transfer by 4 to 5 times [2]. In this paper, the types of concavities configurations and hydrodynamics scale have not been discussed. Apart from the use of artificial roughness elements for heat transfer enhancement in gas turbine blade cooling of power plant engineering, it can also be used for heat transfer enhancement in solar air-heater. Over the last few decades, the world energy demand increases rapidly due to vast growth in the global economy [4]. The enormous world energy demand has been full filled with fossil fuels for a long time. The rate of energy consumption in the year 2018 is twice that of energy consumption in the year 2010 [5]. The increased rate of energy consumption reduces fossil fuel reserves (non-renewable). It causes many environmental issues such as global climate change, air pollution, ozone layer depletion, and acid rain. Due to the increase in energy consumption, the carbon dioxide emission increases to 33.1G tonne in the year 2018, which is the highest rate of carbon dioxide emission till now [5]. Therefore, to overcome all these problems, the creation, development, and deployment of plans for large-scale and carbon-neutral energy production for the present and future are essential. Renewable and sustainable energy sources are promising source of energy to full fill increase energy demand as well as clean environment criteria [5]. Renewable energy sources such as solar, wind, hydropower, and bioenergy can be proved as established power sources that can full fill the increased energy demand if the efficiency of the system is further investigated and improved [5]. Solar energy is considered the most prominent renewable source of energy because the amount of solar flux incident in one hour over the earth's surface is higher as compared to the annual global energy consumption [6]. Solar energy is the cleanest and safest energy source among all renewable sources of energy. Solar energy, which is eco-friendly as well as abundant in nature, is expected to full fill 70% of the world's energy demand by 2100 [7]. So, it is essential to capture solar energy and used it effectively. Two different technologies named solar thermal and photovoltaic are used to harvest solar energy [5]. Photovoltaic technology can able to convert solar energy directly into electricity [5]. Whereas in the case of solar thermal technology, the harvested solar energy is used to heat air, water, and

other fluid [5]. As per the global installed capacity of solar energy, about 70% of solar thermal systems are more popular than PV technologies [5]. Solar air heating system is a widely used solar thermal technology due to its design simplicity and cost-effectiveness [8]. The transportation of solar energy in the form of the electronic wave from the sun to the earth's surface is a continuous process. It is converted into heat and supplied to the flowing fluid before it can be used to dry agricultural cultivated products for space heating and industrial application [9]. This can be done with the help of a solar air heater.

In a flat plate type solar air-heater, the air has to be heated through a rectangular duct below a metal absorber plate. The sun-facing side of the metal plate is painted black to facilitate absorption of solar radiation incidents on it to reduce the thermal losses [9]. There is a significantly lower value of thermal efficiency in solar air-heater. It is mainly because of the low value of the convective heat transfer coefficient between the air and absorber plate. As a result, it leads to high absorber plate temperature and a more significant amount of heat losses to the environment [9]. A laminar sub-layer is developed on the absorber plate's heat transferring surface, which is mainly responsible for the high value of thermal resistance [9]. So, the heat transfer rate can be enhanced by disturbing the layer by introducing artificial roughness [9].

A few review papers are related to the enhancement of heat transfer in a solar air heater using artificial roughness has been carried out. However, all artificial roughened surfaces used for heat transfer enhancement are not addressed in previously reviewed articles, and more significant artificial roughness like dimple has not been reviewed yet. Besides, different arrangement of dimples and their geometry to enhance the heat transfer in various thermal systems has been reviewed [10, 11]. Thus, this study's novelty is a comprehensive review of all roughened surfaces, such as protruded and intended surfaces, which gives a path of selection among the roughened surface for further research in other thermal systems. So, the aim is to enhance the efficiency of the existing system and develop new green technologies. In this present paper, an attempt has been made to categorize and review the reported heat transfer enhancement methods. It includes different heat transfer techniques, the design of an extended surface, and various experimental and numerical approaches to improve heat transfer. Applications of heat transfer techniques have also been reported in the present paper. The reported geometry of artificial roughness in the review paper, which provides maximum heat transfer enhancement and low-pressure drop in the flow channel, can be implemented further to improve heat transfer and the efficiency of the solar air heater. The artificial roughness geometry, which provides the best overall performance, can be incorporated with a solar thermal system with nanofluid to enhance the performance.

HEAT TRANSFER ENHANCEMENT THROUGH INTERFERENCE OF FLOW

Artificial roughness elements such as fixing wires, machining ribs of different shapes, forming dimple/protrusion to enhance the heat flux in a flow channel have been investigated. The literature on applying artificial roughness in the flow channel covers a wide range of roughness geometries for studying heat transfer enhancement rate and friction factor characteristics. These techniques reported by various investigators are described in the following subsections.

Dimple/Protrusion Shaped Geometry

The formation of dimples and protrusion on the flow channel surfaces has been considered a simple and economic methodology. It is the subject of many recent experimental investigations. The heat transfer rate of dimple shape roughness is higher as compared to the smooth surface channel. The pressure loss penalty or friction loss usually does not increase appreciably as compared to other roughened channels. Experimental and numerical investigations are reported in the literature to study heat transfer and friction factor characteristics of dimple/protrusion intended flow channel. The different dimples, such as spherical, cylindrical, teardrop, triangular, V-shaped dimple, elliptical and inclined elliptical, concave, and convex, have been investigated. The geometrical shapes of these dimples are shown in Figure 1(a) to 1(f) [12–15]. Figure 2 shows parameters related to the geometry of the dimple's models [16].

Afanasyev et al. [17] experimentally investigated the friction factor and heat transfer augmentation rate in spherical cavities' intended surface. The flow over the concavities intended surface is considered to be turbulent flow. The experiments have been carried out in a special aerodynamics test bed using a traditional procedure for diagnosing the boundary layer. Ten plates have been taken as prototypes. In 9 plates, the spherical concavities have been intended on the surface in a staggered fashion in different densities and geometrical parameters. The rest of one surface has a smooth surface for the experiment. Heat transfer rate enhanced by 30–40% as there is no breakaway around such relief. There is no appreciable change observed in hydrodynamics flow. Chyu et al. [2] investigated the potential of concavities in heat transfer augmentation from turbine blades/vanes and combustor liners. The flow condition has been considered at high Reynolds numbers than the data published in the Russian report. Two different types of concavities, named hemispherical and teardrop concavities, have been taken for experimentation. The area of inferior heat transfer of hemispherical concavities has been reduced by using teardrop concavities. Sixty test runs have been carried out, out of which 10 test runs have been carried out for single concavity, and the rest 50 test run have been carried out for staggered arranged concavities. The
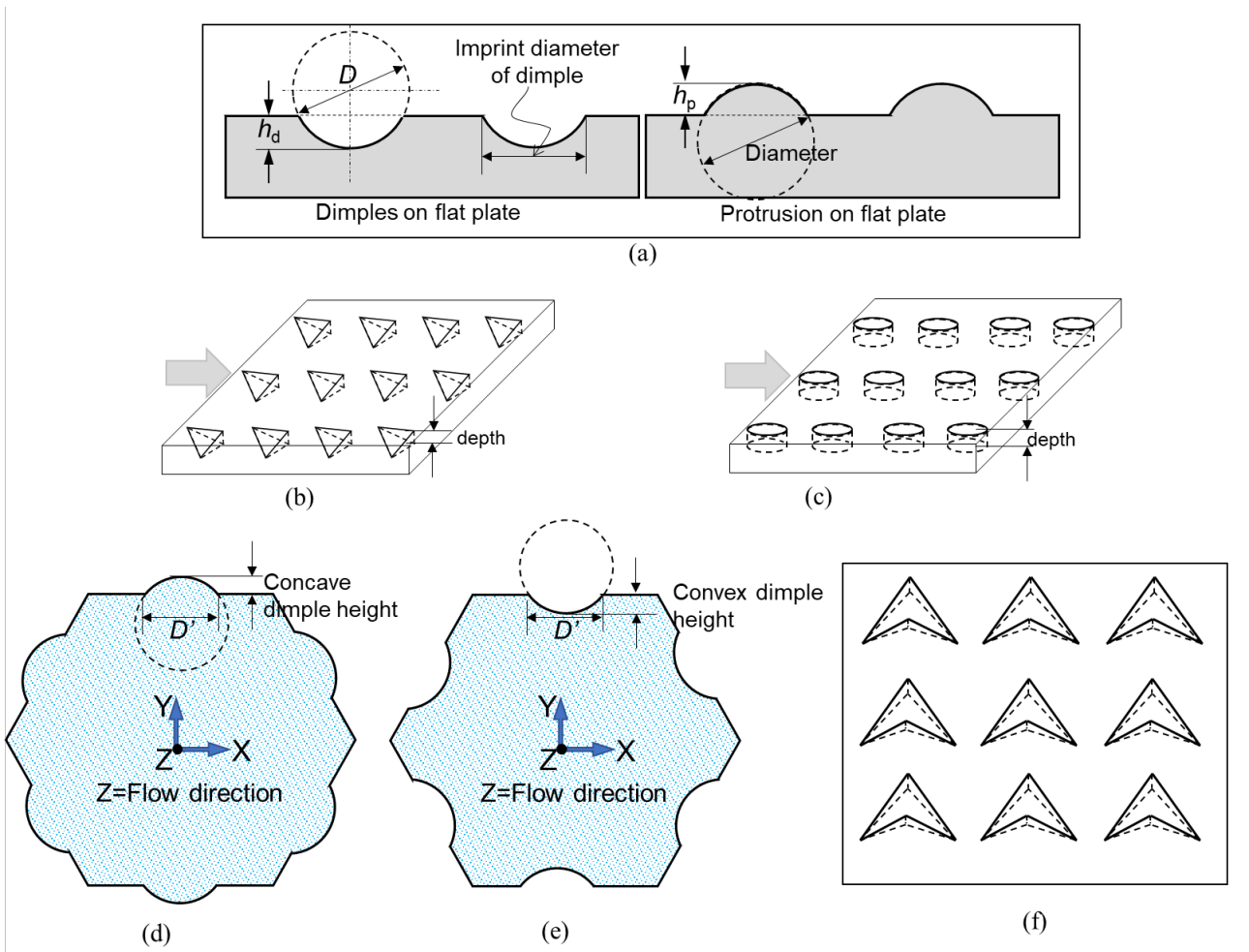
Figure 1. (a) Dimple/Protrusion Geometry, (b) Triangular Dimple, (c) Cylindrical Dimple, (d) Concave Dimple, (e) Convex Dimple and (f) V - shaped Dimple.
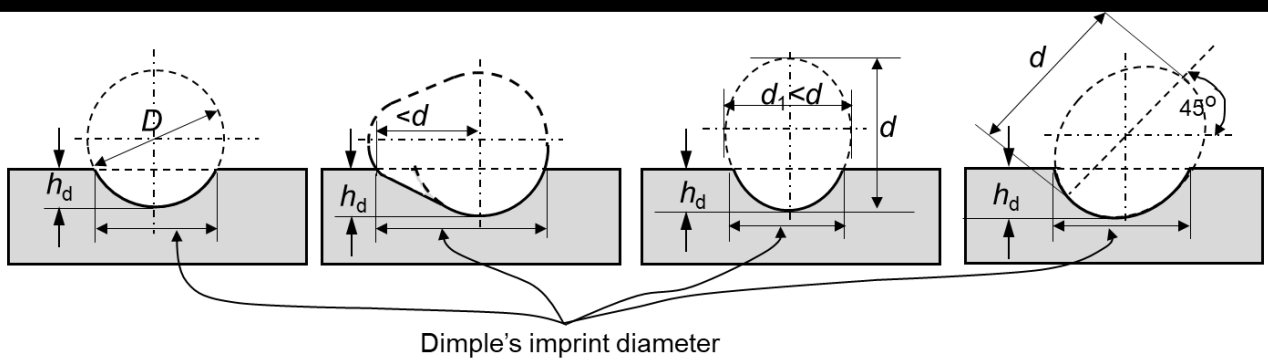

Figure 2. Dimples with different shapes, from left to right indicates; Spherical, Tear Drop, Elliptic and Inclined Elliptical Dimple.

extent of wake spread around the single concavity provides follow-up studies and design guidelines for arrays comprised of multiple concavities. The local heat transfer distribution on the surface roughened with hemispherical and teardrop shape concavities has been measured using a custom-made transient thermochromic liquid crystal imaging system. The vortex burst from the concavity wall enhanced turbulent mixing of bulk flow and enhanced the entire participating wall's heat transfer. However, the tear-drops-shaped concavity intended surface has a high heat

transfer rate compared to the spherical concavity. Both have a similar overall heat transfer rate, and it is 2.5 times the smoother counterpart for the Reynolds number range 10,000≤Re≤ 50,000. The concavities' heat transfer rate is equal to the rib turbulators, but it is less than the broken rib. The pressure loss penalties of both the concavities are less than any protruding element, as shown in Figure 3 [2]. The improvement is nearly by a factor of two in terms of the magnitude of relative pressure co-efficient. Besides cooling, the concavity also reduces weight as well as it is easy to manufacture.

Moon et al. [18] reported the heat transfer coefficient and friction factor of concavities intended surface placed at one wall of the rectangular channel. The heat transfer coefficients have been measured using the thermochromic liquid crystal technique. The possible ratio of channel height to the depth of indentation of the cavity has been taken to investigate its effect: 0.37, 0.74, 1.11, and 1.49. The experimental investigations have been carried for Reynolds numbers range from 12,000 to 60,000. Most heat transfer augmentation occurs in the outside region of concavities. The rates of heat transfer have a higher value downstream at the edges of concavities as compared to upstream of concavity. The heat transfer enhancement of hemispherical concavities' intended channel is constant. It is 2.1 times the smooth surface channel when the H/D ratio varies from 0.37 to 1.49 in a thermally developed flow region. The friction factor of concavity intended surface for the aerodynamically fully developed region is around 0.0412 and it is 1.6 to 2.0 times than the smoother counterpart. The thermal performance of the dimpled surface is higher than the smoother surface. The thermal performance of the dimpled surface is equal to 1.75, whereas the thermal performance of the conventional rib lies between 1.16 and 1.60. The thermal

performance result confirmed that the dimpled surface has high heat transfer capability with less pressure penalty or low-pressure penalty. The channel height in the range 0.37≤H/D≤1.49 neither affects heat transfer coefficient nor friction factor. Mahmood et al. [19] reported instantaneous dynamics and time-averaged characteristics of the vortex structure shed from the dimple placed on one channel wall. The studies have been carried out for 13 rows of staggered arranged concavities in the stream-wise direction where each dimple has an imprint diameter of 5.08 cm and depth to imprint diameter ratio to be maintained at 0.2. The Reynolds number varies concerning the channel heights are from 600 to 11,000 and the channel height to dimple imprint diameter ratio varies as 0.25, 0.5, and 1.0. For all the H/D values, a primary vortex pair is shedding from the central portion of the dimple, including the large up wash region. With the decrease in H/D value, the strength of the primary vortex increases. In addition to that, there is an additional vortex pair induced from the span-wise edges of the dimple. The vortex is shaded from the core of the dimple periodically and continuously and is followed by inflow advection into the concavity to satisfy the continuity. The frequencies of these events occur scale on average bulk velocity and imprint diameter of concavity, which gives non-dimensional frequencies of 2.2 to 3.0 for all H/D values considered. Hill et al. [20] measured experimental results on and above the dimpled surface placed on one wall of the channel for the Reynolds number ranges from 1250 to 61,5000 and the ratio of inlet air stagnation temperature to heated surface temperature varies from 0.68 to 0.94. The relative channel height of 0.5 has been taken for the investigation. The results obtained are flow visualisation, the survey of time-averaged total pressure, stream-wise velocity, spatially resolved local Nusselt number using infrared thermography
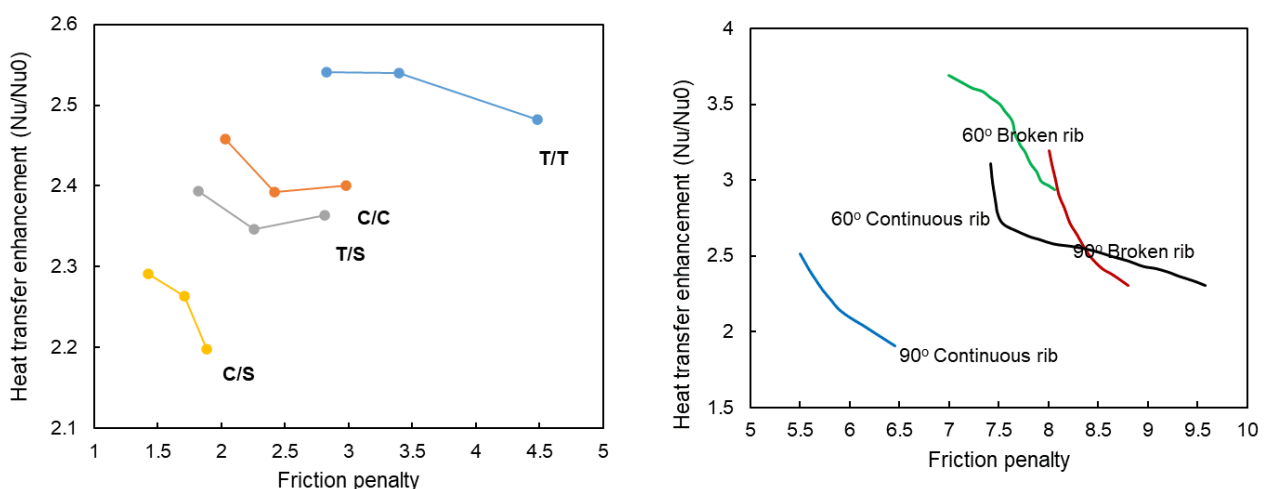

Figure 3. Heat transfer enhancement versus friction penalty, from left to right; heat transfer enhancement at different combinations of surface condition and heat transfer enhancement at continuous and broken ribs.

along with the conjunction of energy balance, thermocouples, and in-situ calibration procedures. Flow visualisation shows vortical fluid and vortex pair shaded from the dimple, including large up wash regions, packets of fluid emanating from the central portion of the dimple, and vortical fluid and vortex structure shaded from the diagonal of the dimple. These vortex structures augment the local Nusselt numbers at the downstream rim of the dimples, both slightly in the depression and flat surface adjacent to the downstream of the dimple. This augmentation spread all over the surface of the dimple and it becomes more pronounced with the decrease of the ratio of air inlet stagnation temperature to heated surface temperature. Hence the local and spatially averaged Nusselt number increases with the decreases in the ratio of inlet air stagnation temperature to surface temperature. This is due to the transmission of vortical fluid by the cool fluid present in the central region of the duct towards the heated dimple surface. Bunker et al. [21] reported heat transfer and friction factor for a fully developed turbulent internal flow in a circular tube with six different concavities surface array geometries. Two different concavity depths and three different concavity array densities have been taken for the test in the bulk flow condition for which the Reynolds number ranges from 20,000 to 90,000. Liquid crystal thermography has been used for the measurement of temperature distribution on the outside of the concavity tubes. Using the averaged heat transfer coefficient value for fully developed flow, the overall heat transfer rate of concavity intended tube surface compared with baseline smooth surface tube. The friction coefficient is also compared with the baseline result. Dimple depth ranging from 0.2 to 0.4 relative to the surface diameter of dimple along with densities of surface area varying from 0.3 to 0.7. Dimples have been arranged in-line fashion. The heat transfer enhancement rate of dimpled surface internal passages is about factor 2 or more than if the relative dimple depth is 0.3 or higher than it and the surface area densities are equal to 0.5 or higher than it. The subsequent friction factor multiplier for this type of configuration is equal to 4 to 6. Vorayos et al. [22] analysed the heat augmentation rate of a flat plate intended with dimples by varying the dimple pitch. For analysing, the heated air has flowed past over the dimple surface flat plate. Hence this is the case of external flow. Two types of dimple arrangements named staggered and in-line have been used for investigation. Fourteen different dimple surface arrangements are obtained by varying ST and SL (the distance between centre of the adjacent dimple in transverse and stream-wise direction, respectively). It is reported that for the staggered arrangement, the maximum Nusselt number is 26% higher than the smoother one. For in-line arrangement, the maximum Nusselt number is 25% higher than the smooth surface. Xie et al. [23] investigated the effect of dimple pitch, depth, and radius on turbulent fluid flow and heat transfer rate for different dimple shapes such as teardrop, spherical and elliptical. It has been obtained from the investigation that the strength and the extent of the recirculation induced in the teardrop increase as compared to the spherical and elliptical dimple, which is the main cause of heat transfer augmentation. In addition to the heat transfer enhancement, the teardrop concavities reduce the pressure loss as it flows smoothly on the streamline of the surface. The Nusselt number and friction factor of the teardrop dimple increases with the increase of dimple depth and radius and decreases with pitch decreases. The enhanced tube with teardrop dimple with D = 2 mm, P = 15 mm, R = 4 mm, and Re = 5000 showed the largest performance evaluation criterion value of about 2.06. Park et al. [13] investigated numerically the heat transfer rate as well as flow characteristics for seven types of dimples imprinted on one wall of the channel using FLUENT. The Realizable k-e turbulence model without wall function has been used to study the flow characteristics numerically. The different dimples such as spherical, cylindrical, and tilted cylindrical, in-line triangular dimple, reverse in-line triangular, staggered triangular dimple, and reversed triangular dimple have been taken for investigation. The high aspect ratio channel (aspect ratio = 8) whose one wall is incorporated with seven different types of concavities has been studied. The turbulent intensity and the Reynolds number value chosen for the study are 0.5% and 12,000, respectively. The data to be measured are spatially averaged Nusselt number, Span-wise normal plane survey of stream-wise velocity, stream-wise vortices, eddy diffusivity for momentum and heat. The results show there is an existence of primary vortex pair at the central region of the dimple and there are two additional vortex pairs at the span-wise edges of the dimples, which augment the magnitudes of eddy diffusivity for momentum and heat in circular types dimple. Advection of reattaching and recirculation flow from the location within the spherical concavity, strong instantaneous vortex flow, mixing of vortex pair is apparent. In all cases of triangular type concavity, there is only one primary circulation zone present within the dimple. As the augmentation of the magnitude of eddy diffusivity for momentum and heat depends on the presence of vortical structure on dimples, only a single primary circulation zone in triangular type dimple gives less heat transfer enhancement rate. The overall thermal performance and most significant local and the overall increase in eddy diffusivity for momentum and heat occurs in spherical and tilted cylinder concavities. Silva et al. [24] investigated both numerically and experimentally the influence of dimple shape and orientation on the heat transfer coefficient of the vortical fin. The published literature review concludes that the thermal performance can be increased by increasing the heat transfer surface area by introducing dimples, increasing the relative dimple depth and relative dimple pitch. The high heat transfer surface area can be obtained by increasing the second half of the dimple (downstream of the dimple), Trailing edge of the dimple, Flat surface adjacent to the downstream rim of the dimple. The

second half, trailing edge and the following proposed solution can augment the flat surface.

(i) Second half of the dimple: Elongating the dimple along the direction of flow

(ii) Trailing edge of the dimple: Elongating trailing edge along the perpendicular direction of the flow, and

(iii) Flat surface adjacent to the downstream rim of the dimple

The above-proposed solution will provide three different shapes of dimple such as oval shape dimple with its long axis oriented parallel to the direction of flow (it is known as horizontal dimple), oval shape dimples whose long axis is perpendicular to the direction of flow (it is known as vortical dimple), double dimple (it is modelled as circular dimple) by introducing a small dimple in the wake region of all the main dimple. Oval dimple can be modelled as circular dimple splits into two circular halves diametrically by a square section. The oval shape dimple is again categorised into an oval shape dimple by varying the distance between the centres of two half-circular dimples. The numerical investigation was carried out by using the commercial computational fluid dynamic code to obtain the optimum configuration of the dimple and both experimental and numerical investigation is carried out for flat surface and dimple surface for comparison purposes only. The boundary condition which is required for the solution are such as the temperature of the air, which is treated as an ideal gas at the entrance is Ti = 300 K and the uniform velocity is 5.6 m/s for a Reynolds number = 500 based on channel height. Heat flux of 21,000 Watt/m^2 has been supplied from the base of the dimpled surfaces. All other surfaces are assumed to be adiabatic with a gap exit modelled as velocity outflow at atmospheric pressure. For numerical simulation, the solver used is segregated implicit with the semi-implicit method for solving the pressure linked equation. The SIMPLE formulation has been used to obtained pressure solution. The upwind scheme has been used for solving momentum and energy equations. The numerical simulation result indicates that the oval shape with its long axis orthogonal to the flow direction provides the best thermal performance; therefore, the overall Nusselt number enhanced by 10.6% for the dimpled imprinted surface. From the numerical simulation result, it is confirmed that the circular dimple provides the best thermal performance as compared to the flat surface. Double dimple and oval shape dimple with its long axis orthogonal to the flow direction will provide better thermal performance than the circular dimples. Thermal and friction losses increase due to the elongation of the dimple. Oval dimple with its long axis in the flow direction showed the worst performance than the circular dimple (close to the flat plate). For the oval dimple imprinted surface, the heat transfer coefficients were improved from 4.5% (Re = 1000) to 11% (Re = 500) with the lower bound range. It

is observed that the improvement in heat transfer rate in the dimple channel depends on the Reynolds number. The values of heat transfer coefficients at Re = 500 was consistently higher than those at Re = 1000. From the experimental result, it is confirmed that the Re = 1000 suggested for laminar regime reduces the heat transfer rate on dimpled surfaces with the increase in Reynolds number as presented in for oval shape dimple-2 plate, heat transfer improvement reduced by 10.4% at Re = 500 and 1.9% at Re = 1000 when the power level is 14%. Whereas the circular plate heat transfer rate was consistently reduced as compared to the flat wall. The increase in the intensity level of turbulence over the dimpled surface is responsible for enhancing the diffusion and reducing the beneficial thermal effects of vortex shading and secondary flow from the dimple. Though the present investigation has been focused on the laminar regime, the heat transfer augmentation in the dimple occurs due to an increase in turbulence level intensity. The intensity of the turbulence level can be increased by increasing the Reynolds number. From the numerical simulation result, it has been concluded that the improvement in the Nusselt number depends on the Reynolds number. The simulation has been based on a laminar viscous model therefore, it is unable to capture the turbulence intensification effect. It has been observed that the average wall temperature of dimple plates after being corrected by the inlet temperature was always equal or lesser than the flat plate temperature. A maximum reduction in the temperature of about 3.7K has been obtained in the oval dimple-2 vortical configuration, which shows the potential benefits of dimples in the laminar flow channel.

The experimental average heat transfer rate for different geometrical model has been presented in Table 1. For oval shape dimple-2 plate, heat transfer improvement reduced by 10.4% at Re = 500 and 1.9% at Re = 1000 when the power level is 14%. Whereas the circular plate heat transfer rate was consistently reduced as compared to the flat wall. The increase in the intensity level of turbulence over the dimple surface is responsible for enhancing the diffusion and reducing the beneficial thermal effects of vortex shading and secondary flow from the dimple. Though the present investigation has been focused on the laminar regime, the heat transfer augmentation in the dimple occurs due to an increase in turbulence level intensity. The intensity of the turbulence level can be increased by increasing the Reynolds number. From the numerical simulation result, it has been concluded that the improvement in Nusselt number depends on the Reynolds number. The simulation has been based on a laminar viscous model therefore, it is unable to capture the turbulence intensification effect. It has been observed that the average wall temperature of dimple plates after being corrected by the inlet temperature was always equal or lesser than the flat plate temperature. A maximum reduction in the temperature of about 3.7 K has been obtained in the oval dimple-2 vortical configuration,

Table 1. Average Heat transfer co-efficient Experimental Results, Re = 500,1000

Model	Power (W/m²)	Re = 500			Re = 1000		
		Average Twall(K)	h (W/m²K)	Nu/Nu0 (h/hflat)	Average Twall(K)	h (W/m²K)	Nu/Nu0 (h/hflat)
Flat	14000	324.01	8.68	—	316.48	12.96	—
Circular	14000	322.14	8.89	1.024	315.47	12.50	0.965
Oval	14000	320.77	9.58	1.104	314.64	13.21	1.019
Flat	21000	336.97	9.01	—	327.15	12.68	—
Circular	21000	335.88	9.00	0.999	325.91	12.53	0.988
Oval	21000	332.50	10.04	1.114	323.60	13.54	1.068

which shows potential benefits of dimples in the laminar flow channel.

Hwang et al. [12] investigated the heat transfer coefficient of various dimple or protrusion (bump) pattern walls in a straight rectangular channel using the transient TLC technique. The dimple or protrusion is placed either on one wall of the channel or on both channel walls. Hence depending upon these arrangements, four different test cases have been obtained. The test duct taken for investigation is 15 mm in height and 105 mm in width. The dimples imprint diameter (hd) or the protrusion height (hp) is equal to 3.75 mm. The aspect ratio (W/H) of the rectangular channel is equal to 7. The hydraulic diameter duct is 26.25 mm; the length of the developing flow channel is 265 mm. The length of the test plate is 190 mm. The test plate is 10 mm thick transparent acryl. There are 12 rows of the dimple/protrusion on the test plate. The dimple/protrusion diameter is 15 mm; the imprint diameter and height for both cases are 12.99 mm and 3.75 mm, respectively. The dimple/protrusion height 3.75 mm is 0.25 D. The rectangular channel height is normalised by dimple height or protrusion height (H/hd or H/hp) is equal to 4. The local heat transfer coefficient inside the dimple or protrusion is measured using the transient TLC technique. The friction factor and performance level also measured for both dimple and protrusion patterned walls. The Reynolds number based on hydraulic diameter (Dh) varies from 1000 to 10,000 from the result obtained, it is concluded that each test case's thermal characteristics and performance level are different. The dimple wall case provides similar thermal characteristics and performance levels for a single dimple wall as well as a double dimple wall. However, the double dimple wall's flow mixing rate is higher compared to the single dimple wall. Hence, the double dimple wall's heat transfer enhancement rate is higher than the single dimple wall. The low heat transfer zone became wider within the dimple with the decrease in Reynolds number and minimum heat transfer co-efficient move towards the downstream direction. The double protrusion wall's heat transfer pattern at a higher Reynolds number takes pea-shape with the decrease in Reynolds number, the heat transfer pattern takes the circular shape. The pea-shape heat transfer patterns appear on the front side of the protrusion and the low heat transfer region occurs at the protrusion's rear side. The double protrusion wall's heat transfer rate is higher because of higher flow acceleration and intense mixing of flow. The heat transfer pattern for both single and double protrusion walls are similar at ReDh = 1000. At lower Reynolds number flow conditions, both double dimple or protrusion wall heat transfer rates are higher. The heat transfer enhancement rate of double protrusion wall or double dimple wall is about 14 and 7, respectively. The heat transfer enhancement rate at higher Reynolds number for both single as well as double protrusion and double dimple is about 2.3, respectively. As the heat transfer rate of both double protrusion and dimple wall is higher; hence its performance level also higher (P.F. = relative Nusselt number ratio/relative friction factor ratio). At Reynolds number 1000, the double protrusion walls and double dimple wall performance level is about 6.5 and 6, respectively. The double protrusion wall's pressure loss is higher due to the decrease in flow cross-sectional area. However, in the dimple wall case for both a single dimple wall and a double dimple wall, pressure loss penalty increment is similar. Silva et al. [25] investigated both experimentally as well as numerically the heat transfer enhancement rate of dimple heat sink supply with laminar airflow. The investigation is carried out for three different types of surfaces flat, circular (spherical) and oval (elliptical/trenched) dimpled indented surface. The flat plate is taken as a baseline for comparison purposes only. The dimples are imprinted on both sides of the copper heat sink. The dimple with relative pitch (S/D) and relative dimple depth of (δ/D) equal to 0.2 was machined on both sides of the copper plates. The air impinges over the leading edge of the plate. The oval dimple with the same relative pitch ratio of S/D = 1.21, dimple depth δ/D of = 0.2 and circular edge to edge distance same as the circular dimples has been taken for investigation. The test plate is placed at the middle of the channel, where a uniform heat flux has been supplied in the in-plane axis of the plate. For both these configurations,

the average heat transfer coefficient and Nusselt number ratio are obtained experimentally. The finding which is obtained after experimentation are: (a) There is an enhancement of heat transfer coefficient for the test plates with the increase of mass flow rate, (b) At low Reynolds numbers (ReH = 500), the relative Nusselt number ratio for both circular as well as oval shape dimple was less than 1.02, (c) The relative Nusselt number ratio for circular as well as oval shape dimple at Reynolds number range from 750 to 1500 ratio has been obtained approximately 1.06 irrespective of ReH. The heat transfer enhancement up to 6% as compared to the flat plate consistently observed for both circular and oval shape dimple when the Reynolds number varies from 500 to 1000. Additionally, pressure drop, flow structure and thermal performance were simulated numerically. The heat transfer coefficient value obtained numerically close to the experimental result for the Reynolds number up to 750. The pressure drop on the dimple surface is either equivalent to or less than the flat plate without the dimple. The simulation result of both circular and oval shape dimple imprinted plates has been analysed. From the result analysis, it has been established that a primary vortex pair has been introduced from the recirculation region present inside of the dimple. The primary vortices have occurred upstream of the dimple. With the increase in airflow, the primary vortices are also elongated in the downstream direction and became stronger. The oval shape dimple plate has higher primary vortices than the circular plate for the same airflow conditions. The secondary vortex flows are generated at each side of the dimples. The phenomenon such as reattachment of the central and secondary vortex flows at the trailing edge region of the dimples responsible for enhancing heat transfer co-efficient in this zone. Burgess et al. [26] studied the friction factor experimentally, local Nusselt number, spatially averaged Nusselt number and globally averaged Nusselt number for a dimpled wall rectangular channel. Experimental results have been measured for the dimpled imprinted on one wall of the widest channel whose aspect ratio is equal to 8. The ratio of channel height to dimple imprint diameter is equalto1.00. The result to be presented for the Reynolds number range from 9940 to74,800, which is based on channel height for a turbulent intensity of 0.033 and ratio of inlet air stagnation temperature to surface temperature 0.93 to 0.94. The experimental result to be collected for the dimple depth to dimple imprint ratio of 0.1, 0.2, 0.3 to present the influence of dimple depth. The effect of Reynolds numbers and stream wise development at δ/D = 0.1 is also investigated. The data will be collected at the same dimple imprint diameter, dimple spacing, channel aspect ratio, same channel height to dimple imprint ratio, and the same thermal boundary condition. At all Reynolds numbers, local and spatially averaged Nusselt number increases with the increase in dimple depth (δ/D) from 0.1 to 0.3 (all other experimental and geometrical parameters are held constant). This is due to the following factors: (a) deeper

dimple produces the strength and intensity of vortices and associated secondary flow ejected from the dimples and (b) Increase in the magnitude of 3D turbulence production and turbulence transport level. The effect of these phenomena is clearly evident in the local Nusselt distribution inside the dimple and span-wise edges of the downstream rim of the dimple. The result shows that for δ/D = 0.3 there is two local maxima, whereas for δ/D = 0.1 and 0.2 only one local maxima. By varying δ/D ratio, the different values of normalised Nusselt number have been obtained due to the presence of important phenomenon such as vortex shading of different strength as well as due to shear layer formation, shear layer development and flow reattachment. The shear layer, which forms on the top of the dimples, is stronger and pronounced reattachment of these layers occurred for the deep dimple. For δ/D = 0.3 the shear layer reattachment is slightly farther upstream than the shallow dimple δ/D = 0.2. The zone of shear layer reattachment changes periodically with δ/D values in phase with the sequence of vortex pair shading and flow in rush to the dimples. Due to the continuous vortex shading from the dimple and flow inrush to the dimple, a larger volume of fluid periodically flows into the deep dimple and comes out of the dimple as compared to the shallow dimple. Therefore, a strong vortex pair with a more pronounced secondary flow is generated in the deeper dimple. The net result is an increased ratio of Nusselt number for the flat surface just downstream of the deeper dimples as δ/D increase. There is an increase in friction factor with the rise in δ/D value. The friction factor at δ/D = 0.1 with varying the Reynolds number value from 9940 to 74,800 remains approximately constant. The variation of local Nusselt number value is significant at different stream wise locations. The variation of local Nusselt number concerning Reynolds number is mainly evident on flat surfaces just downstream of individual dimples. Small et al. [27] studied experimentally and numerically the thermal performance of the heat sink incorporated with dimple and bump (protrusion). In a design competition at Carnegie Mellon University, the mechanical students designed and manufactured 27 numbers of heat sinks used in mock processors to enhance the heat transfer rate. The heat sink is manufactured with design constraints on total volume and dimensions. Keeping the size of the heat sink constant and the height of the fin constant by varying the number of fins and arrangement, the thermal performance of the heat sink is evaluated. For these two types of arrangement known as staggered and inline is used. Here the different dimple arrangements such as heat sink with D/D (both sides imprinted with a dimple) and D/B (one side imprinted with dimple and other side incorporated with the bump or protrusion) is also investigated. The thermal fluid behaviour of the heat sink with dimple and without dimple is measured and the experimental result is compared with the simulated result. The dimples which are introduced in fins are spherical as well as a cylindrical dimple.

The variety of heat sink with different numbers of fins, staggered, in-line dimple fins, bumps fins, plain fins have been taken for simulation. The heat sink total volume is maintained to be constant at 80 cm³ that is equal to the volume of the original heat sink. The uniform velocity of air maintained as 4 m/sec and temperature maintained as 20°C at the inlet throughout the simulation. From the experimental result and numerical simulation result, it is concluded that the dimple enhances the thermal performance of the heat sink but at a significant amount of pressure drop. The optimum number of fins that provide the best thermal performance is different for staggered and inline arrangements. For inline fin arrangement, the number fin present in each row are 999 (that means each row contains 9 number of fins) for this 999 heat sink, the two different cases can be considered one is both sides with dimple and other one is one side with dimple and other side is plain. For both these arrangements, the thermal resistance and pressure drops are very close. However, heat sink 999 with one side dimple and the other side bump provide lower thermal resistance and higher pressure drops. The staggered arranged heat sink fin is 989, in which in one row there are 9 numbers of fins, in the second row 8 number of fins and in the third row again 9 numbers of fins. There are also two possible cases; one is fins are imprinted on both sides with a dimple (D/D) and the other is imprinted with dimple and other is incorporated with the bump (D/B). In both cases, the pressure drop and thermal resistance are not slightly different from those of heat sink with plain fins. Staggered arranged fin heat sink because higher pressure drops lower thermal resistance. Inline fin with one side imprinted dimple and other with bump delivers lower thermal resistance and higher-pressure drops comparing with those with plain and fin imprinted on both sides with the dimple. The heat sink with staggered arranged fin (989) intended with the dimple on one surface arranged in three rows gives the best thermal performance with 25% less set value of volume. From the observations, it is clear that dimple fin heat sink enhances the heat transfer rate at the price of increasing pressure drops. The mechanism which is responsible for the augmentation of heat transfer rate in dimple surface channel is: (a) the unsteadiness in the flow structure which is ejected periodically from the dimple and rushed into the dimple, (b) The reattaching of the shear layer, which forms at the top of the dimple and (c) The vortical and vortices which is continuously shaded from the dimple. A 999 heat sink with a spherical bump with the same dimension as the dimple is simulated and the result concluded that the spherical bump has an adverse effect on thermal performance and pressure drop. One problem of fins with spherical dimples is manufacturing difficulty. A 999 heat sink with dimple/bump increases the pressure drop as well as thermal resistance. It is evident that an optimum number of fins are required for best thermal performance provided the volume of the heat sink need to remain constant. However, the optimum number of fins required to get the best heat transfer behaviour in dimple fins and plain fins where heat sinks are different. For dimple fin heat sink, the optimum number of fins required to get the best heat transfer behaviour is 989 and for plain fin heat sink, the optimum number fins required to get the best heat transfer rate is 878. For inline arrangement, the optimum numbers of fins required to get best transfer behaviour by dimple fin heat sink are 999 and for plain fin heat sink is 888, respectively. From the simulation and experimental results, it is confirmed that the bump fin produces higher thermal resistance and pressure drop compared to the plain fin heat sink. Elyyan et al. [28] studied numerically the unsteady flow structure, heat transfer and friction factor in a channel whose one wall is imprinted with dimple and the other one is incorporated by the protrusion. To visualize the flow in a channel the large eddy simulation is carried out. Dimple imprint diameter D = 2.0 and dimple depth is 0.4. Dimple/protrusion pitches in span wise and stream wise direction are equal to P = S = 3.24. Dimple and protrusion are staggered without any offset concerning each other. Both wall surfaces are heated by supplying a constant heat flux boundary condition. The domain is periodic in both stream wise as well as span wise direction. The boundary condition such as No-slip boundary condition and constant heat flux boundary condition has been applied to the channel surfaces (dimple and protrusion surfaces). Non- dimensional incompressible time-dependent Navier-Stoke equation and energy equation is solved using a generalised coordinate system considering the boundary layer is fully developed thermally as well as hydrodynamically. The governing equation for momentum and energy can be discretised using a conservative finite-volume formulation and a second-order central scheme on a non-staggered grid topology. The simulation is carried out for the Reynolds numbers value 220,940 and 9300. Where ReH = 220 (represent laminar flow). ReH = 940 represent the weak turbulent flow and ReH = 9300 represent fully turbulent. The Reynolds number value chosen are based on channel height. The turbulence generated by the separated shear layer position on the upstream rim of the dimple was responsible for heat transfer augmentation in the dimple. The vortex shaded from the shear layer moves to the downstream half, reattach with the surface and augment heat transfer. Flow ejected from the dimple cavity get turbulence (small vertices) along the side and downstream of the dimple rim at a higher Reynolds number. The formation of turbulence in the dimple rim and ejection of the same out of the cavity augment heat transfer on the flat surface immediately downstream of the dimple cavity. As the heat transfer augmentation depends on the turbulence generation; hence the use of the low Reynolds number flow is not viable. The unset of unsteadiness is responsible for the augmentation of heat transfer and can be controlled by the dimple geometry. On the other hand, in protrusion the heat transfer augmentation is due to flow

impingement and flow acceleration between the protrusions. The generation of turbulence in the separated shear layer and wake of the protrusion influences heat transfer augmentation on the flat surface adjacent to the downstream of the protrusion. Despite the lesser dependence of protrusion on turbulence generation, they too do not seem viable as heat transfer augmented surfaces in the steady laminar regime. At ReH = 220, the protrusion has less Nusselt number value as compared to the flat surface and it is due to the low momentum wake of protrusion on surface heat transfer. However, the dimpled surface shows some augmentation but the use of dimples and protrusion for flow at low Reynolds number, which is not viable. When the Reynolds number reaches 940 the flow is no longer laminar and it exhibits turbulent like characteristics, but the flow is not fully turbulent. At this Reynolds, the protrusion exhibits a high heat transfer coefficient as compared to the dimpled surface. This is due to the flow impingement on the protrusion surface and flow acceleration between the protrusions. The overall Nusselt number augmentation as compared to the smooth laminar channel is about 2.94. When the flow is fully turbulent heat transfer rate is augmented by the same magnitude on both sides of the channel and there is an overall augmentation of 2.53 based on the turbulent baseline co- relation. At a low and medium-range of Reynolds number, both dimple and protrusion exhibit the same pressure loss penalty. Whereas at ReH = 9300 the dimpled surface contributes a higher-pressure loss penalty and comes in the form of drag. The overall form drags increases by 44% at ReH = 220 and 80% at ReH = 9300. The dimple's overall form drag predominates the protrusions. The overall friction co-efficient augmentation rate is a function of the Reynolds number. The overall friction co-efficient augmentation rate at low Reynolds ranges from 1.67 to a high value at the highest Reynolds number. Shin et al. [29] investigated the heat transfer coefficient of a channel whose one wall is imprinted with the dimple. The spherical type dimples are fabricated on one wall of the channel. The diameter of the spherical dimple is 16 mm and dimple depth is about 4 mm. Two channel heights of 0.6 D and 1.2 D are taken for investigation. Two different types of dimple configurations known as sparse and dense are taken for study. The space between two adjacent dimples for sparse and dense dimple configuration is 2 D and 1.1 D, respectively. The dimples are arranged in a staggered fashion and the Reynolds number based on the channel hydraulic diameter varied from 30,000 to 50,000. The transient liquid crystal technique is used for heat transfer measurement. Various flow phenomena are introduced by the dimple. The boundary layer of the main stream separated when it enters the dimple and produces a recirculation zone on the upstream side of the dimples. The main stream flow, which is separated, reattaches in the downstream side of the dimple surfaces. This same reattached flow form twin vortex flow. These complex phenomena are responsible for high and low heat transfer in and near the dimples. From the experimental data, it is observed that the overall Nusselt number increases with the increases of Reynolds number for lower channel height cases for the same Reynolds number, the overall Nusselt number of Height channel height also increases. The higher Nusselt number value in lower channel height is due to an increase in flow disturbances. With the decrease in channel height to dimple diameter ratio, the disturbance in the flow increases by the dimples as a result of which a higher Nusselt number value is obtained. The high and low heat transfer region occurs in and downstream of the dimple to the complex phenomena induced in the dimple such as flow separation, recirculation, and reattachment. In the upstream of the dimples, heat transfer coefficients are low due to the presence of the flow recirculation region. The heat transfer co-efficient downstream of the dimples is higher because of the flow attachment. High heat transfer coefficient along the edges of the dimple and it is about 2/3 of the upstream edge of the dimple. It has been observed that the formation of twin vortices and flow reattachment of the high heat transfer zone exists along the rim of the dimple. When the flow is ejected out from the dimple and the flow reattaches again on the flat surface, which is immediately adjacent to the downstream rim of the dimple causes a high heat transfer region. The distribution pattern of the overall Nusselt number for both densely and sparsely arranged dimples is same. The Nusselt number value obtained for densely arranged dimples is higher than that of the sparsely arranged dimple at the same Reynolds number and channel height. With the decrease in distance between two adjacent dimples, more flow disturbance is introduced by the dimple, which results in an enhancement of heat transfer. The averaged Nusselt number on the dimpled surface compared to a smooth tube with the same hydraulic diameter. The highest Nusselt number ratio is obtained for the densely disturbed dimples with a low channel height. The actual pressure loss penalty is higher for the higher Reynolds number case, but the friction factor ratio difference is not significant. The thermal performance factor, which is the ratio between the ratios of Nusselt number of friction factor, decreases as the Reynolds number increases. The thermal performance factor depends more on the arrangement of the dimples and the channel height to dimple diameter ratio or the arrangement of the dimple. Dimple depth is also a key parameter for augmentation of heat transfer rate. Belenkiy et al. [30] described the heat transfer intensification in the tube surface, which is attached with a straggled arranged concave cavity in the internal tubular passages. From the investigation, it is concluded that it is used generally in shell and tube heat exchanger. The heat transfer enhancement rate for deep concavities is about 2.5 times and for shallow indentation, it is about 2 times the smooth counterpart. High-pressure loss occurs in the internal tubular passages incorporated with concavities. Chuskin et al. [31] illustrated the flow of heat transfer agent around

spherical concavities and self-organising vortex flow coming out from the concavities in the form of jets and intensive mass transports from the surface into the main core of the flow. Intensive mass transport by the heat transfer agent from near the wall region to the outer region reduces the thermal resistance in the heating surface as the boundary layer thickness decreases. Hence the convective heat transfer increases. Lin et al. [1] investigated the 3D flow computationally in a hemispherical concavity and heat transfer rate in a high aspect ratio duct. The channel one wall or both walls have been roughened with hemispherical concavities in a staggered fashion. Four rows of hemispherical concavities arranged in staggered fashion have been studied for Reynolds number values Re = 23,000 and Re = 46,000. The computational studies have been based on the Ensemble-Averaged of conservation of equation of mass, momentum and energy, which are closed by low Reynolds numbers shear stress transport k-omega turbulence model (wall function are not used). Solutions were generated by a finite volume method, third-order accurate flux difference splitting of Roe with limiters, multigrid acceleration of a diagonalised ADI scheme with local time stepping, and patched/overlapped structured grids. From Numerical simulation, it is found that once the flow enters into the concavity, it forms two vortical structure and it comes out from the cavity in two different from the downstream cavity centre the vortical structure emerges out as a single bundle tube and another way it will emerge out from the concavity in a zigzag fashion separately. These flow features have significant effects on enhancing surface transfer. Huang et al. [32] studied the heat transfer enhancement rate of the heat sink with jet impingement introducing dimpled numerically. The microchannel heat sink with dimpled is compared with the microchannel heat sink with jet impingement without the dimple. Different dimples like concave, convex, mixed dimple are incorporated with heat transfer surface area of a microchannel heat sink with jet impingement. The microchannel heat sink with impinging jet having convex dimple exhibited the best cooling performance. It provides less flow resistance in MIJS. Among the entire dimple MIJ the convex dimple provides the best overall performance followed by MIJS without dimple, with mixed dimple and with the concave dimples. Zhou et al. [33] studied mass and heat transfer rate using the Naphthalene sublimation method for square internal passage whose one wall is intended with four different dimples named square, triangular, circular and teardrop shape dimple. The experimental result is obtained using Naphthalene sublimation method and the computational result is obtained using FLUENT. The measurement is carried out at Reynolds number (Re) = 21,000. The numerical simulation is carried out for the same flow conditions (Re = 21,000) and for the same geometry used for experimentation. The computation is performed with FLUENT version 5. By considering the symmetry condition, only half of the dimple channel is

simulated to reduce the computation time. The meshing of the computational domain has been carried out using GAMBIT. Fine meshes have been generated inside the dimples and around the dimples to determine essential features in the vicinity of the dimple. The problem has been modelled as a steady 3-dimensional heat transfer problem with uniform wall temperature. The Reynolds Stress Model has been employed for calculation during computation of solid walls such as the bottom of the dimple. Two smooth sidewalls are set to the same wall temperature. The uniform inlet velocity from the inlet Reynolds number = 21,000. The main flow temperature is set to be at 293K and the wall temperature is set to be 323K. As the temperature difference between the main flow and wall is only 30K hence the uniform velocity at the inlet is very low (it is less than 10 m/s). Hence it is considered that the velocity field is independent of the temperature. First, the velocity field is computed when the steady-state velocity is obtained the temperature field calculation is done. The temperature field is calculated with a constant Prandtl number assumption. The Sherwood number is obtained both inside of the dimple and around the dimple. Flow patterns and heat transfer distribution for four different types of dimples are obtained. From the experimental and numerical results, it is cleared that teardrop shape dimples provide the highest heat and mass transfer among all the four types of dimple. In the wake region, the triangular dimple shows the lowest value of Nu/Nu0, while the circular and teardrop shape dimple shows comparable. The highest to lowest Nusselt number value sequence obtained are teardrop shape, circular shape, square shape and triangular shape dimple. The flow pattern obtained from numerical simulation on one side of the symmetry line for four different type dimples predicted a counter-rotating vortex pair for a triangular dimple. For the circular and tear drop shape dimple, a single vortex roll is observed in the wake. There is no noticeable vortex roll observed for the square dimple in the wake region. The predicted Nu/Nu0 in the wake shows a peak along the path of the wake vortex. A higher value of Nu/Nu0 (peak value is >4.8) is found within the narrow band on the downstream edges of the four dimples. The value of Nu/Nu0 decay rapidly over a distance of one dimple length in the wake of dimple from 2 to 1.2. Inside the dimple, lower Nu/Nu0 values are seen along the upstream of the dimple floor. In the upstream, the value varies from 0.4 to 1, while the higher Nu/Nu0 is found in the downstream portion of the dimple bottom (values in the range 1–3). The experimental Sh/Sh0 shows similar behaviour around the dimple perimeter. The Nu/Nu0 varies in the range of 1.3 to 1.7. Chang et al. [14] investigated the detailed Nusselt number distribution, area-averaged Nusselt number, pressure drop coefficient for hexagonal duct intended centrally with one column of three different types of dimple. The three different types of dimple arrangement used for investigation are convex-convex, concave-concave and con cave-convex. The effect of dimple

configuration as well as, Reynolds number on Nusselt number distribution, pressure drop coefficient over developed flow region has also been investigated. The Reynolds at which the investigation has been carried out are Re = 1200, Re = 5000, Re = 20,000 and Re = 30,000. The overall performance of both smooth and dimple intended hexagonal duct has been studied and compared. The included angel of hexagonal duct diverts the trajectory of the dimple induced vortical structures between the two adjoining polygonal walls. Due to which the dimple duct requires the higher flow momentum indexed by Re to simulate the local heat transfer enhancement impact on the apex of each convex and concave dimple. Hence the critical Reynolds number value at which the Nusselt number peaks start emerging at the centre of the convex and concave dimple are higher as compared to the rectangular duct whose opposite walls are incorporated with dimple. The relative Nusselt number ratio (Nudimple/Nusmooth) increases for all dimple configurations to levels ranging from 2.8 to 5.9 and 2.5 to 1.5 for laminar and turbulent flow, respectively. The ratio between the average Nusselt number of dimples intended hexagonal and of the smooth hexagonal channel first increases then start decreases with the increases in Reynolds number for both laminar and turbulent flow condition. When 900≤Re≤30,000, the pressure drops penalties increase to the levels of 2 to 6.7 and 2.5 to 3.6 for laminar and turbulent flow conditions in dimple intended hexagonal duct. The separated flow tripped by the convex dimple induced a higher heat transfer enhancement rate than the vortical structure induced by the concave dimple, due to which the area- averaged Nusselt number of the convex-convex dimpled intended hexagonal duct will be higher as compared to the other. The averaged Nusselt number will follow the order convex-convex concave-convex (convex) concave-convex (concave) concave- concave. The overall performance of the convex-convex dimple incorporated hexagonal duct is higher as compared to others. Slabaugh et al. [34] discussed the heat transfer augmentation through the fully developed region of a narrow rectangular channel of aspect ratio 2 whose bottom wall has been imprinted with the dimple. Three different types of dimples named as small dimple, large dimple and double dimple have been imprinted on the bottom wall of the rectangular channel. The investigation has been carried out at channel Reynolds number 20,000,30,000 and 40,000. The effect of dimple configuration on flow structure, which helps to improves advection of heat away from the wall has also been investigated. The local heat transfer coefficient distributions, channel-averaged Nusselt number augmentation and overall friction augmentation throughout the length of the duct to evaluate the performance of dimples have been studied. At Re = 20,000, the distribution of heat transfer coefficient is relatively uniform in the large dimple. The heat transfer rate in the downstream edge of the dimple is higher as the stagnation streamlines intersect the wall. With the increase

in Reynolds number the non- uniformity in the distribution of heat transfer coefficient increased. It is primarily due to variation in convection heat transfer in the stagnation and recirculation zone present within the dimple. In the recirculation zone, the heat transfer rate is low as the flow in recirculation pockets heated up to the wall temperature and the driving temperature difference causing the flow of heat is reduced. The bottom wall is imprinted with increased size dimples and the participating surfaces within the dimple have high performance. The strength and development of turbulence in the channel by the dimple feature increased. The heat transfer rate increased with the increase in Reynolds number. At Re = 20,000 and 30,000, the small dimple's recirculation zone is higher due to which the heat transfer rate of the small dimple is less compared to the large dimple. Whereas at Re = 40,000, the dimple's performance improves due to the reduction of the recirculation zone. At Re = 40,000, the recirculation zone is reduced by half of the size that is introduced at Re = 20,000. The downstream advection of turbulent eddies stimulate convection heat transfer over the wall is significant in the regions of high convection coefficient immediately downstream of each dimple. The double dimple is the amalgamation of two small dimples machined in pair with the centre-to-centre distance less than the dimple imprint diameter. In double dimples, it is observed that the recirculation zone reduced to a very small percentage of overall dimples surface area, which is much less than the recirculation zone introduced in the single dimple. Hence, there is high heat transfer uniformity as well as overall high performance of the channel. At Re = 20,000, there is an augmentation of heat transfer at the dimple's downstream edge. At this Reynolds number on the top and sidewall where dimples are not featured, there is no apparent augmentation in Nusselt number. This is due to the availability of less kinetic energy in the mainstream flow, which is responsible for the augmentation of heat transfer rate. As the Reynolds increased, the turbulence of intensity of flow is increased and the heat transfer performance of the side and top wall is increased. The top wall's heat transfer rate is higher than the sidewall through the fully developed portion at Re = 30,000 and 40,000. At Re = 40,000, double dimple promotes significant gains in surface Nusselt number on the channel's bottom wall. In double dimple first dimple exhibits, stagnation-recirculation characteristics and the second dimple use the increased turbulent kinetic energy to enhance convection heat transfer from its own wall and then further promote increased vortex generation to be swept downstream. The averaged Nusselt number of the double dimples is on the levels of large dimples and around 25% higher than that of the small dimple. The friction factor is decreasing with the increase in Reynolds number. Raoetal. [35] investigated experimentally as well as numerically the influence of dimple depth on the pressure loss penalty and heat transfer characteristics in a pin fin-dimple channel where dimples are located

transversely between the pin fins. The investigations have been carried out in the Reynolds number range of 8200 to 50500 for different dimple to diameter ratios. There were 10 rows of pin-fin dimple combined structure where the transverse spacing to diameter ratio S/D = 2.5, pin fins the stream wise spacing to diameter ratio X/D = 2.5, the pin fin height to diameter H/D = 1.0 have been maintained for investigation. The dimples print diameter are same with the pin fins has been maintained. The numerical analysis has been done using commercial solver fluent 6.3. The unstructured hybrid mesh has been generated for all computational domains using GAMBIT software. Denser grid type mesh has been used in the flow region nearer to the wall. A periodic pin fin dimple channel segment has been studied considering the periodic condition in the flow channel. The computation has been carried out considering heat transfer occurs to the solid wall and in the fluid. The bottom wall of channel has been supplied with constant heat flux, whereas the channel's top wall has been taken as adiabatic. The no-slip boundary condition has been applied to the channel pin fin and dimpled surfaces. At the channel's inlet and outlet, pair of periodic boundary conditions has been employed stream wisely for the velocities, pressure, and temperature. The computation has been done using realizable k-ϵ turbulence model. Throughout the investigation, two assumptions were used; (i) in compressible fluid and (ii) the equations related to the flow field and energy were used uncoupled. The numerical errors have been minimised by the method of a second-order volume discretisation. In the numerical analysis; pressure-velocity coupling has been modelled using SIMPLEC algorithm. All predicted quantities have been taken at steady state. The minimum convergence criteria for the continuity equation and energy equation, velocity and turbulence quantities are 10^{-4} and 10^{-7}. At δ/D = 0.3 the pin fin dimple channel showed the highest friction factor in the Reynolds range 8200 to 50500, which are higher than the pin fin channel by about 5.3%. The pin fin dimple showed relatively lower pressure loss at δ/D = 0.1 and 0.2 for the same Reynolds number range than the pin fin channel. At δ/D = 0.1 and 0.2 the pin fin dimple showed 17.6% and 14% lower pressure loss than the pin fin channel. At δ/D = 0.1 the pin fin dimple showed lowest friction factor. It has been reported from numerical investigation, at δ/D = 0.1 and 0.2 lower pressure loss and friction factor than pin fin channel and at δ/D = 0.3 higher pressure loss and friction factor than pin fin channel within the studied Reynolds number range. With the increase in dimple depth, the turbulence level in the mainstream flow region is especially decreased, whereas the intensity of turbulence in the near-wall flow region downstream the dimple is distinctively increased. Phenomenon such as flow separation and recirculation are the reason for the reduction in rate of turbulent mixing in the upstream half of the dimple. Due to flow reattachment in the downstream half of the dimple and flow impingement at the rear rim of the dimple, the

turbulent mixing rate is apparently increased. Therefore, there is an increase in pressure loss penalty in the pin fin dimple channel. The Nusselt number value of pin fin dimple channel at δ/D = 0.2 is 8% higher and at δ/D = 0.3 is 19–14% higher than the pin fin channel when the Reynolds number ranges from 8200 to 50500. The Numerical analysis shows that the Nusselt number is about 1.1%, 8.0%, and 11.4% higher than that of the pin fin channel. Overall thermal performance parameters of the pin fin channel and the pin fin dimple channel decreases with the Reynolds number. At δ/D = 0.3 and 0.2 the overall thermal performance increased by 14.9% to 12.7%, which is higher than the pin fin channel, respectively. Rao et al. [16] investigated both experimentally and numerically the effect of dimples geometries on the heat transfer rate and flow friction associate with the turbulent flow over dimple surfaces. Three different dimples with equal depth, such as spherical, teardrop, elliptical, and inclined elliptical, have been taken for investigation. The friction factor, heat transfer and flow characteristics in a cooling channel imprinted with different dimples shapes have been investigated. The obtained results were compared with each other for Reynolds number ranging from 8500 to 60000. The Nusselt number of all the dimple intended channel increased with the Reynolds number. The Nusselt number ratios of the entire dimpled channel were approximately independent of Reynolds number (for Re > 18700). The Nusselt number value of spherical dimple ranges from 42.1 to 226.0, which is 1.5 to 1.7 times, then the Nusselt number value obtained for fully turbulent flow in a smooth channel. The teardrop dimple Nusselt number is 18% higher than the spherical dimple, which is 1.8 to 2.0 times the fully developed turbulent flow in the smooth channel. The elliptical shape dimple showed 9.3% lower Nusselt number as compared to the spherical dimple. The inclined dimple imprinted channel exhibits approximately the same value of Nusselt number with the spherical intended channel over the study range of Reynolds number. The teardrop dimple showed the highest Nusselt numbers among all the four dimple shapes. The changes in the shape of the dimple from teardrop to elliptical leads to an apparent decreased in the rate of heat transfer 28.0%. The Nusselt values of the teardrop dimples at Re = 50,500 is about 13.0% higher and 8.2% lower than the spherical dimples, respectively. And similar observations have been found for elliptical dimples. Due to flow separation and recirculation for all dimples, the upstream half of the dimpled wall showed a lower heat transfer rate. The rate of heat transfer by convection mode is enhanced in the downstream half of the dimpled wall as well as in the downstream area of the dimples, especially near the rear rim of the dimples. The vortex flow shedding from the dimples increased the turbulent mixing rate in the near-wall flow region. In those areas, the friction factor approximately remains constant with the increase in Reynolds number however the friction factor ratio increased. The spherical dimple channel friction factor

varied from 0.04 to 0.043 in the studied range of Reynolds. The spherical dimple channel friction factor is 1.2 to 2.0 times the friction factor of fully developed turbulent flow in a smooth channel. The friction factors of both elliptical and inclined elliptical dimple channel are approximately as for the spherical one. With the increase in Reynolds number the friction factor increases. Therefore, the friction factor of the tear drop dimple has been increased by 1.6 to 2.3 times of the smooth channel and it is about 35–15% higher than the channel with spherical dimples. The heat transfer rate deteriorates in all dimple channels due to the presence of flow separation and flow recirculation in the upstream half of the dimples. There are flow reattachment and impingement onto the downstream half of the dimple wall. The heat transfer enhancement occurred due to vortex shedding from the dimples especially near the rim of the dimples. Two strong symmetrical vortex flows especially in the left and right half of the dimples and vortex shedding along the diagonals of the dimples introduced due to flow across the teardrop dimples. The vortex after generation is injected into the neighbouring downstream half of the dimples. Such types of oscillating vortex flow patterns continue throughout the flow length. Therefore, there is a significant improvement in 3D turbulent mixing in the near-wall flow region. Due to the enhancement in turbulent mixing rate, the overall heat transfer augmentation was carried out significantly. The flow separation and recirculation in teardrop dimples are less as compared to spherical dimples Due to the presence of a straight sloped wall in the upstream half of the dimples. The existence of a large flow recirculation zone and a more steep flow separation zone in the elliptical dimple responsible for low heat transfer performance. The presence of phenomena such as asymmetrical vortex flow structures in the inclined elliptical dimples and the large up washing flow region in the trailing edge of the dimple promotes flow reattachment. Therefore, the heat transfer enhancement rate on the downstream half of the dimple is higher than the upstream half of the dimple. The teardrop dimples showed the highest thermal performance of about 1.8. The teardrop dimple is about 11% higher thermal performance than the spherical dimples. The thermal performance of the inclined elliptical dimple is approximately the same as the spherical dimple. The elliptical dimples showed lower thermal performance and it was about 16-10% lower than the spherical dimples. Rao et al. [36] studied experimentally as well as numerically the heat transfer rate of turbulence flow channel whose one wall has been intended with arrays of spherical and teardrop dimples. The dimple depth to diameter ratio is same as the depth of dimple and it is 0.2. The heat transfer as well as flow structure characteristics in two different channels have been investigated and compared to each other for the Reynolds range of 8500–60,000. The computation of flow structure and heat transfer characteristics has been investigated using commercial software ANSYS FLUENT 14.5. A structural

hexahedral meshing has been generated using commercial software GAMBIT for all computational domains. The near wall flow region of the computational domain has been meshed with denser grids. The channel's bottom wall has been supplied with constant heat flux and the top wall of the channel has been insulated. The no-slip boundary condition has been applied to both top and bottom wall of the channel. At the inlet of the channel, the inlet velocity boundary condition and at the outlet of the channel pressure outlet boundary condition have been used to predict heat transfer and pressure loss in the dimple channel. The assumptions taken for investigation are: (i) the fluid is incompressible (ii) constant thermal properties of the fluid (iii) the flow field and the energy equations were uncoupled. As second order up wind volume discretisation scheme was used for the energy equation and SIMPLEC algorithm has been used for pressure velocity coupling in the computations to reduce the numerical errors. The minimum convergence criteria for the continuity equation, velocity and turbulence quantities are 10^{-5} and 10^{-8} for the energy equation. The averaged heat transfer enhancement of spherical dimple showed 1.5 to 1.7 times and friction factor 1.2 to 2.0 times then the fully developed turbulent flow in a smooth circular duct. The teardrop dimples showed the heat transfer enhancement of 1.8 to 2.0 times and friction factor of1.6 to 2.3 times then the fully developed flow in a smooth circular duct. The teardrop dimple heat transfer enhancement is 18% higher than the spherical dimple as illustrated in Figure 4 [36]. The friction factor is about 35% to 15% higher than the spherical dimple. The overall performance factor of teardrop dimple is higher as compared to spherical dimple as the heat transfer enhancement rate of teardrop dimple is higher as shown in Figure 4 [36]. Due to the enlargement of the heat transfer surface area, the
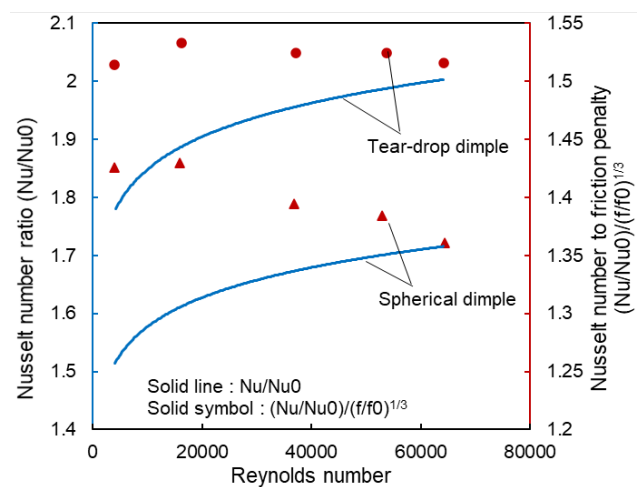

Figure 4. In primary vertical axis: Heat transfer enhancement of dimpled channel and in secondary vertical axis: Overall performance of dimple channels.

teardrop dimple's heat transfer rate was about 1.64 to 1.85 and spherical 2.0 to 2.2 times then the fully developed smooth circular duct. From the numerical simulation result, it has been observed that the turbulent mixing rate for both spherical as well as teardrop dimple increases significantly due to the production of different vortex flow structures. The teardrop dimple produced less flow separation and recirculation in the upstream half of the dimples. In a larger area of near wall flow region of teardrop dimple turbulent mixing rate is higher. Therefore, the local and overall heat transfer rate for teardrop dimple is superior.

Xie et al. [37] investigated the flow and heat transfer characteristics of teardrop dimple/protrusion with different eccentricities numerically and compared with hemispherical dimple/protrusion. The investigation has been carried out for the Reynolds number range 700 to 9000. Four different ratios of eccentricities to the hydraulic diameter such as 0.1, 0.2, 0.3 and 0.4 have been taken to investigate flow structure and heat transfer characteristics. The finite volume method has been adopted for the solution of mass, momentum and energy equations. The upwind scheme with second order accuracy has been used to discretize the convection term and the central difference scheme with second order accuracy for the discretisation of the diffusion term. The SIMPLEC method has been used for the pressure velocity coupling and the realizable k-ϵ model with enhanced wall function. The Nusselt number ratio monotonously decreases as Re increases and it increases from –0.4 to 4 for teardrop protrusion. When the eccentricity increases, the impingement area on to protrusion gets larger as eccentricity increases, the low-temperature fluid covers a more heated surface due to which the heat transfer rate is enhanced efficiently. The heat transfer rate increased by 5% to 10% compared with hemispherical protrusion. Flow covers the teardrop surface easily and impinges on to the rear section with more energy in the teardrop dimple/protrusion. The ratio of Nusselt number decreased when e/Dh varied from 0 to 0.1 and it increased when it is larger than 0.1 for teardrop dimple. The ratio of friction factor decreased with Reynolds when e/Dh < 0.2 and it had not changed much when e/Dh = 0.2 and decreased when e/Dh > 0.2. Thermal performance increased gradually as the centre moves downwards for the teardrop protrusion. The thermal performance value showed minimum value when e/Dh = 0.1 and increased as e/Dh > 0.1 for teardrop dimple. The thermal performance showed the maximum value for teardrop dimple and protrusion when e/Dh = 0.4. Jordan et al. [15] investigated the detailed Nusselt number ratio distribution experimentally for a channel intended with an array of V-shaped dimples. The V-shaped dimple of δ/D = 0.30(δ = dimple depth and D = dimple diameter), which is derived from a traditional hemispherical dimple array arranged in in-line pattern. The V-shaped dimple spacing has been maintained 3.2D in both stream wise and span wise directions. The investigation has been carried out for

the channel Reynolds number ranges from 10,000 to 40,000. The detailed Nu number ratios have been obtained using both a transient liquid crystal technique and a transient sensitive point technique. At a low Reynolds number, most of the heat transfer occurred outside of the dimple as the coolant reattaches to the surface downstream of the dimple. The heat transfer enhancement increased inside the dimple at high Reynolds number (Re = 30,000 to 40,000). The increase in Nusselt number ratios due to increase in momentum associated with the flow at high Reynolds numbers. Higher momentum induced strong counter rotating vortices within the secondary flow inside the dimples. Such vortices produce a high heat transfer coefficient along the trailing edge and downstream of the dimple. Three pairs of counter rotating vortices are formed inside the channel as a result of the corresponding three rows of dimples. The counter rotating vortices pull the flow into the dimple and cause the flow to reattach inside of the downstream edge of the dimple. As the Reynolds number within the channel increases, the thermal performance also increases. Relative to V-ribs, the V-dimple channel produced less loss of pressure. Jing et al. [38] investigated numerically the turbulent flow and heat transfer performance of dimple/protrusion arranged in a rectangular channel with working fluid supercritical carbon dioxide and air. The investigations have been carried out using Reynolds Averaged Navier's Stokes and Realizable k-ϵ turbulence model. The detailed study of Nusselt number distribution, the flow resistance f and the comprehensive thermal performance have been carried out at Re = 90,000. Periodic boundary conditions have been set at the inlet and outlet of the channel for analysis. The air temperature at the inlet is ambient air temperature and pressure is atmospheric pressure. The mass flow rate has been taken as per the Reynolds number 90,000. The side wall has been supplied with a constant heat flux of 1500 W/m². Pressure-velocity coupling scheme SIMPLEC has been adopted and to reduce numerical error, the second order spatial discretisation technique has been used. The fluid separates in the leading edge of the dimple and is attached in the trailing edge. The fluid crashes in the leading edge for protrusion and separates in the trailing edge with the formation of a symmetrical separation bubble. The temperature at the leading edge is higher than the trailing edge in the case of a dimple. The supercritical carbon dioxide has a larger small temperature region and a lower higher temperature region than the air case. The Nusselt number ratio of supercritical carbon dioxide is 2.3 times higher than air at Re = 90,000. The friction factor ratio is close to the air at Re = 90,000. The comprehensive thermal performance of supercritical carbon dioxide is 2.4 times ten the air at Re = 90,000. Saini et al. [39] investigated the effect of roughness and operating parameters such as relative roughness height, relative pitch on heat transfer and friction factor for a solar air heater. The dimple is intended on the absorber plate. The investigation is carried out in the range of Reynolds

number (Re) from 2000 to 12,000, relative roughness height (e/D, where e is the roughness height and D is the equivalent diameter) from 0.018 to 0.037 and relative pitch (P/e where P is the pitch of the dimple) from 8 to12. The roughness height taken for investigation are 0.8, 1.3, 1.5, 1.7 and different pitch value taken are 12, 15, 18 mm and pitch diameter taken are 0.8, 1.3, 1.5 and 1.7 mm. The Nusselt number value as a function of Reynolds number for relative pitch (P/e) values of 8, 10 and 12 and a fixed value of roughness height (e/D) of 0.0322 have been investigated. From experimental data, it is confirmed that the Nu number increases for relative roughness pitch (P/e) of 10 due to separation of the flow at the dimple reattachment of the free shear layer occurs for (P/e) of 10 and maximum heat transfer coefficient occurs in the vicinity of the reattachment region. For relative pitch of 8 and 12 reattachment may not occurs; hence the heat transfer coefficient value is minimum corresponds to these values of P/e. The larger relative roughness height (e/D) produces more reattachment of free shear layer hence the maximum value of heat transfer is found to be corresponding to relative roughness height (e/D) of 0.0379. The friction factor decreases monotonously with the increase Reynolds number for all roughness parameters. The maximum value of Nu number has been found out corresponds to relative roughness height (e/D) of 0.0379 and relative pitch (P/e) of 10. While the minimum value of the friction factor has been found corresponding to relative roughness height (e/D) of 0.02989 and relative pitch (P/e) of 10. Schukin et al. [3] studied the heat transfer and have flow phenomena of single hemispherical cavities in a flat diffuser experimentally. The diffuser angle was θ/2 = 0°, 3.5°, 6°and 8.5°. The cavity diameter has been maintained at 50 mm. At the downstream of the hemispherical cavity, the average heat transfer increased compared to the channel without a cavity. The total heat flow on the inner surface of a hemispherical cavity depends on the mainstream turbulence of flow. Mahmood et al. [40] investigated local and spatially averaged Nusselt number for the dimple surface channel in which opposite wall both with and without protrusion and the shape of the protrusion is same. The protrusions have been arranged without offset with a dimple (configuration-1) and offset with a dimple (configuration-2). The channel aspect ratio has been maintained at 16 and the channel height to dimple imprint diameter ratio has been maintained at 0.5 for investigation. The Reynolds number based on the channel height ranges from 5×10^3 to 3.5×10^4. The inlet stagnation temperature to wall temperature ratio for the channel varies from 0.73 to 0.94. The region of high local Nu/Nu0 results from the collection of vortex pairs and vortical fluid, which are shed periodically from each dimple. This periodically takes the form of repeated cycles of events where each cycle consists of inrush of fluid to each dimple followed by outflow and vortex shedding. The channel whose bottom wall is imprinted with dimple produces lower Nu number ratio values in the upstream

half and higher values in the downstream half of the dimple. The highest values are obtained near the downstream rims of each dimple and on the flat surface adjacent to the downstream of each dimple. At the same Reynolds number and temperature ratio, the ratio of local Nu number of concave cavities intended channel is higher than the smooth channel. The heat transfer augmentation occurs near the downstream rims of the dimple and flat surface adjacent to the downstream and between dimples are due to factors such as: (i) The secondary fluid motions of these vortex pairs near the surface. (ii) The periodicity and unsteadiness of these vortical fluids. (iii) The reattachment of the separated shear layer, which advects across the opening of each dimple. (iv) Augmented turbulence transport. For the top protruded wall and bottom dimple wall channel, the secondary flows ejected in the channel in stronger magnitudes over large portions of the channel cross-sections. The intensities of turbulence and mixing rate are also higher at much lower Renumbers. The obstructions produced by the top wall protrusions and the resulting effects of continuity cause the flow to be forced from the dimples. Due to protrusion, this phenomenon occurs with more violence and over great volumes. With the decrease in the ratio of inlet air stagnation temperature to the wall's surface temperature, the cooler part has higher Nu/Nu0 on the test surface intensifies, broaden and extends farther away from the downstream rims of the dimples. This Nusselt number ratio becomes more significant with the decrease in temperature ratios as the vortex pairs and vortical fluid in a channel bring a large amount of cooler fluid near the dimpled surface from the central parts of the channel. This process is supported by variable property influences and the bouncy effect. Globally averaged Nu number ratio for the protruded top wall and dimple bottom wall channel decreases as the Reynolds increases. The globally averaged Nu number changes about 20% as ReH ranges from 5×10^5 to 4×10^4. The dimple-protrusion surface arrangement channel globally averaged Nu number has a great dependence on Reynolds number than the smooth surface channel. The magnitude of globally averaged Nu number value for protrusion dimple arrangement with an offset higher than without offset. The thermal performance of protruded top wall and bottom dimple wall channel ranges from 1.45 to1.55 and it increases slightly with Reynolds number. The decrease in the magnitude of the protruded top wall's thermal performance is due to a large increase in friction factor ratio (f/f0) caused by protrusion form drag. Mahmood et al. [41] studied experimentally the effect of aspect ratio, temperature ratio, Reynolds number and flow structure on the heat transfer rate of dimple wall channel. The investigations have been carried out in a channel whose one wall has been imprinted with dimple and other wall has been smooth to evaluate the influence of Reynolds number the Reynolds number varied from 600 to 11,000. The inlet air stagnation temperature to wall surface temperature varied as 0.78 to

0.94. The ratio of channel height to dimple diameter (H/D) has been varied as 0.20, 0.25, 0.50 and 1. The ratio of dimple depth to dimple imprint diameter has been taken as 0.2. From the flow visualisation smoke pattern, it has been observed the vortex pair, which has been periodically shaded from the dimple, becomes stronger with the decrease in H/D ratio. The increase of vortex pair shedding caused Nu number augmentation. The Nu number enhancement occurred near the downstream rim of each dimple and flat surface adjacent to the dimple's downstream rim. The local Nu number increased with the decrease in the ratio of inlet air stagnation temperature to the surface temperature of the wall. It occurred due to the bouncy effect and variable property influence. These effects help in the advection of colder fluid from the central region of the channel near to the heated surface. Park et al. [42] studied the flow structure numerically in a channel whose one wall was imprinted with the deep dimple. The dimple depth to dimple imprint diameter ratio $\delta/D = 0.3$ has been taken for the prediction of flow structure. Spherical dimples were intended in a staggered fashion on one wall of the channel. The channel height and dimple imprint diameter both were same and equal to 0.0508 m and the dimple depth has to be maintained at 0.01524 m. The channel height to dimple imprint diameter ratio (H/D) of 1.0 has been maintained for investigation. The hydraulic diameter of the channel has been maintained at 0.0942 m. The uniform velocity profile has been applied at the entrance of the smooth part of the channel. The turbulence intensity of either 0.5% or 15% has been maintained. The dimple imprinted surface has been supplied with a constant heat flux of 940 W/m^2. The ideal gas has been taken as a working fluid with a constant thermal conductivity of 0.0242 W/m-K, a constant absolute viscosity of 1.91×10^{-05} kg/s-m and a constant molecular Prandtl number of 0.794. The nominal value of statistic density was 0.99 kg/m^3. All the investigations have been carried out at ReH of 2700, 12,000 and 41,000. The spatially averaged channel velocities based on Reynolds number were 1.00, 4.43, 6.35 and 17.5 m/s. The numerical analysis has been taken using FLUENT numerical code version 6.0.12 and GAMBIT version 2.0.4 has been used for the development of a computational hexahedral grid. The realizable k-ϵ turbulence model has been used due to improved predictive capabilities in complex flow regions close to the surface. The semi-implicit method for pressure linked equations (SIMPLE) has been used. In order to reduce numerical errors, second order discretisation scheme has been used. The upstream half of each dimple contains the central vortex pair, which is developed in the flow recirculation zone. The vortices of opposite sign contain by recirculation fluid regions on each span wise side. After the fluid advected outside of each dimple, the vortex pair development and structure are tied to the motion of the flow toward and away from the flat surface where the latter has been due to the ejection of flow from the dimple. The vortices

concentrations associated with the central vortex pair is pounced in the region where the eddy diffusivity for momentum and heat are augmented. These characteristics are due to (i) The generation and mixing of strong instantaneous secondary flows with vortex pairs, (ii) The advective transmission of reattaching and recirculation flow from locations within the dimple cavities, and (iii) The vortices which develops in the flow as it turns and advects past the sharp dimple rim. Perwez et al. [43] studied numerically and experimentally the Nu number and pressure loss performance of spherical dimple and inclined teardrop dimple heat sink under different flow conditions. The investigation has been carried out at Reynolds number ranges1800 to 7000. The spherical and inclined teardrop dimple intended on both sides of the heat sink has maintained an equal longitudinal spacing of 10 mm and transverse spacing of 5 mm. The dimple depth to dimple diameter ratio has been maintained at 0.2. The ANSYS FLUENT software version 14.0 has been used for numerical analysis. The complex vortex flow conditions can be predicted efficiently using RNG k-ϵ turbulence models. SIMPLEC technique has been used for pressure velocity coupling. The Navier's stoke equations as well as energy equation, have been used for numerical analysis. The convective heat transfer coefficient increased with the increase in Reynolds number, due to which the Nusselt number increased. The spherical dimple intended heat sink Nusselt number varied from 22.10 to 44.86. The inclined tear drop imprinted heat sink Nu number varied from 23.05 to 47.39. The Nu number value of the plate heat sink varied from 20.24 to 44.10. The teardrop imprinted heat sink Nusselt number was about 8.6% higher than the spherical dimple intended heat sink and 12.99% higher than the flat heat sink. The Nusselt number ratio of spherical dimple incorporated heat sinks has been varied from 1.04 to 1.08 times and the value of inclined teardrop dimple incorporated heat sink has been varied from 1.09 to 1.14 times as compared to the flat heat sink. The friction factor of the spherical dimple imprinted heat sink varied from 0.09 to 0.37 and the friction factor of inclined tear drop dimple imprinted heat sink varied from 0.10 to 0.39. The friction factor ratio of the spherical imprinted heat sink was 1.07 to 1.20 times and the inclined tear drop dimple intended heat sink was 1.12 to 1.26 times as compared to the flat heat sink. The inclined tear drops dimple imprinted heat sink showed the highest thermal performance and it was 7.36% higher than the spherical dimple heat sink. From the flow structure visualisation, it has been confirmed that stronger and larger recirculation regions exist for inclined teardrop dimple heat sink as compared to the spherical dimple heat sink. The inclined tear drop dimple incorporated heat sink exhibits a higher heat transfer rate than the spherical dimple incorporated heat sink. The presence of vortices at downstream of the dimple is responsible for the augmentation of the heat transfer rate. The flow reattachment improves the local heat transfer performance. Silva et al. [44] studied the

flow structure numerically and the heat transfer enhancement rate of dimple intended heat sinks in microelectronic cooling. There are two different types of design that have been taken for investigation. The old design has 9 × 13 arrays of dimple and in the new design it is 11 × 135 arrays. The old design dimple depth has to be maintained at 1.016 mm and dimple imprint diameter has to be maintained at 5.08 mm. The relative dimple depth ratio has been maintained at 0.2 mm and the dimple spacing to be maintained at 0.73 mm. The new design has 11 × 135 arrays of dimple. The dimple depth has been maintained at 0.15 mm. The relative dimple depth has to be maintained at 0.2 and dimple diameter has been maintained at 0.75 mm. The gap between consecutive rows and columns centre lines has been maintained at 0.91 mm. The numerical analysis has been done using FLUENT6.2.16. The grids used were hexahedral/wedge mesh with a cylindrical array of elements within the dimples. The solvers used were segregated implicit, with SIMPLE formulation for pressure solution and upwind scheme for momentum and energy equation. Heat flux employed to the dimpled surface has been maintained to a constant value of 100 W/m². All other wall was presumed to be thermally insulated. The inlet air temperature has been maintained at 300K. The outlet condition was specified as an outflow at atmospheric pressure. The thermal coefficient value of the new design observed to be slightly lower, reaching a maximum of 1.8, whereas for the old design, it was 2.0. In the new design, due to increased spacing between the dimples, the higher thermal coefficient of the land area covers more surface area rendering an average Nu number ratio of 1.67. The new design was 1.2% better than the old model. There is a pressure drop of 12.6% compared to the original array. The overall performance of the old design was about 1.19, whereas the new design showed 1.38. The heat transfer rate of dimple imprinted heat sink was enhanced by 2.5 times the flat surface heat transfer rate. It has been reported that the heat transfer rate independent of Reynolds number in the laminar and transition flow regime. Friction factor increased with Reynolds number. At a low Reynolds number, the overall performance of dimples was higher and friction losses were small. At relative dimple depth to imprint diameter (δ/D) of 0.2 maximum heat transfer occurred by the dimple. The points which are to be considered to enhance the overall performance of the dimple intended heat sink are enlisted as follows: (i) Dimple depth should be maintained equal or less than channel height to avoid stretching of the vortex structure that improves mixing, (ii)The channel height whose opposite walls are imprinted with dimple should be two times of dimple depth or higher, (iii)Dimple spacing should be optimised to take advantage of the thermal coefficient in the flat area downstream from the dimple while keeping the number of dimples to a minimum. Wie et al. [45] studied numerically steady laminar flow and heat transfer inside a rectangular microchannel whose bottom wall was imprinted

with a hemispherical dimple. The rectangular microchannel depth has been maintained at 50 × 10⁻⁶ m and width 200 × 10⁻⁶ m. The dimples have been imprinted in a single row on the bottom surface of the channel maintained pitch at150 × 10⁻⁶ m. The dimple depth and dimple imprinted diameter have been maintained at 20 × 10⁻⁶ m and 98 × 10⁻⁶ m, respectively. The gap between the centres of the dimple maintained is 150 × 10⁻⁶ m. The periodic boundary conditions have been employed for the thermal field at the inlet and outlet. The dimpled surface has been supplied with constant heat flux. Symmetry boundary conditions have been imposed at the centre of the channel. The commercial code FLUENT version 5.5 has been used to solve the periodic flow and heat transfer problem. The grids have been generated using T-Grid scheme for the dimple section and the cooper scheme for the channel section. From the flow structure, it has been observed that streamlines were separated near the upstream corner of the dimple. A separated and recirculation flow region has occurred within the dimple, which spread in most parts of the upstream half and part of the downstream half of the dimple. The reattachment regions occurred at the downstream part of the dimple in the vicinity of the right dimple edges. The heat transfer has been enhanced at all dimple locations. The maximum enhancements have been observed near the downstream edge of the dimple. The minimum enhancement has been observed inside of the dimple at a location that is slightly upstream of the dimple centre. The higher heat transfer region near the downstream edge of the dimple is due to reattachment of the shear layer and extra advection induced by the secondary flow associated with the vortices which are shed from the dimples. With the increase in Reynolds number, the thermal performance parameter's magnitude increases. The spatially averaged Nu number ratios as well as friction factors both increase with the increase in Reynolds number. The microchannel with laminar flow condition showed thermal performance slightly smaller than the microchannel turbulent flow condition. Pressure drops in the microchannel with laminar flow conditions either equivalent to or less than values produced in a smooth channel with no dimple. Woei et al. [46] investigated heat transfer rate experimentally over a convex-dimpled surface of impinging jet-array with three eccentricities E/H (where E = eccentricity between the jet centre and dimple centre, H = jet-to-jet space) between the jet centre and dimple centre. The variation in heat transfer rate due to adjustment of jet Reynolds number (Re) and separation distance S/Dj (where S is the separation distance between the dimpled surface and jet surface, Dj = diameter of the jet nozzle for baseline array) have been investigated. The investigation has been carried out over the Reynolds number ranges of 5000≤Re≤15,000 and over the S/Dj ranges 0.5≤S/Dj≤11. The study has been carried out with three different eccentricities such as E/H = 0, 1/4 and 1/2. The jet diameter and H/Dj have to be maintained at 3 mm

and 4 mm. From the investigation, it has been confirmed that the adequate selection of Reynolds number, S/Dj, the moderated jet to jet interface, shrinkage of inter jet region and elevation of heat transfer in stagnation regions helps to improve uniform heat transfer over the convex–dimpled surface. The increase in Reynolds number value and a decrease in S/Dj value enhanced the heat transfer rate from the dimple surface. When the Reynolds number (Re) ≥ 10,000 and S/Dj = 1.5 the Nusselt number level in the inter jet regions over the convex-dimpled surface with E/H = 0 and E/H=1/4 are less than the smooth-walled surface. The area-averaged Nusselt number of the central jet region (NUC⁻ = A{S/Dj}×Re^{B(S/Dj)}) depends on Reynolds number. The area-averaged Nusselt number of central jet region highest for E/H = 1/2. For asymmetrical surface arrangement (E/H = 1/2 and E/H = 1/4) each jet issued from the orifice plate is bent toward the dimple centre so that its stagnation point is horizontally shifted about 0.5 jet diameter towards the dimple centre. The growing rate of inter jet impacts on heat transfer impediments via increasing Reynolds for convex-dimpled surface appears to be faster than that for the smooth-walled surface. Xie et al. [47] studied numerically different shapes of surface dimples to evaluate the most optimum configurations to augment heat transfer rate from the surface at the expense of less pressure drop penalties. To evaluate the optimal configuration six different dimple shape have been taken for study such as spherical dimple, ellipse-spherical dimple (with its long axis parallel to the flow direction), ellipse-spherical dimple (with its long axis perpendicular to the flow direction), two egg spherical dimple arrangements with the half ellipse with longer axis pointed both away and towards the bulk flow directions and super spherical-dimple. The dimple arrays were aligned with each other as they were located on one surface of square cross section channel in six different stream wise rows. The rectangular channel has been maintained a height of 15 mm and a width of 105 mm. The aspect ratio (W/H) of the test duct has been maintained at 7 with duct hydraulic diameter (Dh) of 26.25 mm. The test plate has been arranged with 12 rows of dimple in a staggered fashion. A total 56 number of dimples have been imprinted on the test surface. For all six different dimple equal depth of 5 mm has been maintained and the average radius of imprint diameter area has been maintained approximately 10 mm. The investigation has been carried out at the Reynolds ranges of 8000 to 24,000. The numerical analysis has been carried out using commercial FLUENT software of version 12.1. ICEM software of version 12.1 has been used for geometry generation, geometry import and mesh generation. The inlet and outlet extension of the channel have been presumed to be adiabatic. A constant surface heat flux of 1000W/m² has been employed in the middle part where dimples have been intended. The no-slip velocity conditions have been applied at all the walls. Uniform velocity related to Reynolds number has been set and the

temperature has been fixed at 300K. The intensity of turbulence has been set at 5%. The fluid has been presumed to be incompressible with constant thermal properties. The different turbulence model such as RNG k-ε model, the standard k-ε model, the Reynolds stress model, SST k-ω model and the υ2f model has been used to simulate 3D turbulent flow and heat transfer in five different dimples imprinted duct. The pressure and velocity fields coupling have been carried out using SIMPLE algorithm. The fully developed turbulent flow channel incorporated with six different dimples has a higher heat transfer rate as compared to the fully developed turbulent flow smooth channel. The heat transfer augmentation rate of spherical dimple intended channel varied between 1.747 to 1.906, for elliptical dimple intended channel where the long axis aligned to the direction of flow and orthogonal to the flow direction varied from 1.745 to 1.907 and 1.753 to 1.950, respectively. The heat transfer augmentation rate of the super elliptical dimple intended channel varied from 1.721 to 1.903. The channel with egg-shaped spherical dimple with half longer axis pointed both away and towards the bulk flow direction heat transfer augmentation rate varied from 1.745 to1.907 and 1.742 to 1.899, respectively. The dimple shapes which showed the best overall thermal performance were spherical indentation and the ellipse spherical, where the long axis orthogonal to the direction of bulk flows. The ellipse spherical showed best overall performance at relatively lower Reynolds range, whereas the spherical indentation channel showed best overall performance at higher Reynolds range. The spherical ellipse dimples whose long axis orthogonal to flow direction have higher shear layer reattachment over downstream portions. The transition of surface geometry of dimple plays an important role in heat transfer augmentation. Similarly, heat transfer augmentation also depends on the diameters of surface curvature. The surface shape with more significant discontinuities decreases the thermal performance, whereas if the local surface curvature diameters are too small, the thermal performance also decreases. The sensitiveness of these configurations increases with the Reynolds number. The spherical indentations dimple has the largest constant curvature diameter, due to which it produces better thermal performance at a higher Reynolds number. The ellipse spherical dimple, with its long axis orthogonal to the direction of flow, has minimum surface discontinuities with continuous dimple shape curvature. It provides a relatively higher overall thermal performance at a lower range of Reynolds numbers. The averaged Nusselt number predicted using RNG k-ε model is 58.45 and experimentally, it is 53.29. From the result analysis, it has been concluded that Nu number obtained numerically closer to experimental. Xie et al. [48] investigated numerically the heat transfer enhancement rate and pressure loss penalty in a two-pass channel with 180° turn incorporated with pins, dimples and protrusion. The investigation has been carried out for the Reynolds Number ranges from 100,000 to

600,000. Arrays of circular pins have been mounted on the tip. The pins have been arranged in a staggered fashion. The pins have a height of 8.128 mm and a diameter of 4.064 mm. In the stream wise and span wise direction, the pitch has to be maintained at 21.117 mm and 12.19 2 mm, respectively. A total of 165 numbers of pin fins have been attached to the channel. At the dimpled tip channel, arrays of dimples are intended on the internal tip- cap. The dimples have a depth of 2.032 mm and a print diameter of 4.064 mm. In the protruded-tip channel, an array of protrusions has been protruded on the internal tip-cap. The numerical simulation has been carried out using fluent Software of version 6.3.26. The generation of the computational model and the grid generation in the computational domain have been carried out using GAMBIT software of version 2.4.6. The k-ϵ turbulence model used for measurement of three-dimensional flows in a two-pass channel incorporated with pins/dimples/protrusions. The pressure and velocity coupling have been carried out using SIMPLEC algorithm. Constant heat flux has been supplied on the bottom wall and the other walls have been presumed to be insulated. No-slip boundary conditions have been implemented to each and every wall. Uniform velocity at a temperature of 300K has been maintained at the inlet and an outlet flow condition has been imposed at the outlet. The fluid which has been presumed to be incompressible throughout the flow has constant thermal physical properties. The Realizable k-ϵ model with standard wall function has been applied on the walls for the near-wall treatment because of high Reynolds numbers and complex models. The minimum convergence criterion for continuity, momentum and k-ϵ equations has been taken as 10^{-4} and for energy equation it has been taken as 10^{-7}. When the fluid turns through 180°, arises centrifugal force and pressure difference from the curvature. It helps to originate a pair of counter-rotating vortices in turn. These vortices are significantly strong and responsible for the transmission of cold fluid from the centre towards the outer wall. The pins, dimples or protrusions force the vortices towards the tip-wall and thereby improve the turbulent mixing of the approaching cold fluid and hot fluid near the tip. It has been observed that the high temperature occurred at the side corner where recirculation flow occurred. It has been concluded that the tip with pins/ dimples/protrusions has high heat transfer augmentation as compared to the smooth tip channel. It has been enhanced by a factor up to 3.0 times (pins) and 2.0 times (dimple/ protrusion) compared to the smooth tip channel. The usage of pins/dimples or protrusions enhanced heat transfer by a substantial amount at low additional pressure loss. The pinned-tip channel's pressure loss penalty is 2–5% higher than the smooth tip channel, whereas dimpled-tip or protrusion-tip channels are 2–10% higher. The pressure loss penalty is much less than the increased heat transfer rate, especially at a low range of Reynolds number. The addition of pins/dimples or protrusion to the tip of the two-pass

channel increased weight. The added weight induces large stress, resulting in the reduction of the channel's reliability and life. As per the consideration of the added weight ratio, it has been found that the dimple-tip has the best thermal performance. It has been concluded that the use of dimples in tip cooling is an effective way when mechanical stress is critical. The Nu number ratio (Nu/Nu0) decreased and the friction factor ratio (f/f0) increased with the increase in Reynolds number. A smooth tip two-pass fully developed channel heat transfer increment rate has been varied from 1.07 to 1.25. The heat transfer varied between 1.43 and 2.63 for an augmented tip two-pass channel. The friction factor of the smooth tip channel and the augmented tip channels over the fully developed varied from 4.2 to 5.2 and 4.5 to 5.9, respectively. Elyyan et al. [49] studied numerically heat transfer and pressure drop characteristics of fin banks imprinted with dimple and protrusion using direct and large eddy simulation. The investigation has been carried out over a Reynolds number range Re H = 200 to 15,000. The heat transfer and pressure drop characteristics have been evaluated for laminar, transition and fully turbulent regimes. For the investigation, the same imprint pattern with two different fin pitches has been considered. The fin comprises two parallel plates with staggered dimples and protrusion on opposite walls without any offset with respect to each other. As per two different fin pitches, two different cases have been investigated. In case - 1, pitches along the stream wise as well as span wise direction have to be maintained at 1.62 and the dimple/protrusion imprint diameter with dimple depth has to be maintained at 1.0 and 0.2, respectively. In case-2 the pitch, dimple/protrusion diameter, depth has to be doubled. A hybrid structured/unstructured multi-block grid has been used to discretize the computational domain. Constant heat flux boundary conditions have been imposed on both the channel walls. Case-1 produced little or no heat transfer augmentation in the steady laminar regime up to ReH = 900. Case - 2 showed some augmentation in the steady laminar regimes, which has been last up to ReH = 450. At low Reynolds regime ReH < 1000, case - 2 showed superior heat transfer rate. At ReH =3000, when the flow becomes turbulent, there is no difference in heat transfer augmentation rate. The heat transfer augmentation on the dimpled surface is caused by vortex impingement in the cavity's reattachment region. The ejection and redirection of these vortices and additional vortex shaded at the dimple's rim, responsible for the high heat transfer rate on the flat region adjacent to the downstream rim. In the case of protrusion, flow impingement and acceleration between protrusions have been played an important role in the enhancement of heat transfer. In the case of a low Reynolds number, higher friction loss is exhibited than the case-1. However, the high friction loss difference decreased in the fully turbulent regime. In both cases, the form drag is about 80% of the total losses when the Reynolds number increased to fully turbulent

flow. Wang et al. [50] numerically studied the effect of angle of convergence on flow structure as well as on heat transfer rate of a pin fin wedged duct imprinted with hemispherical dimple/protrusions. The investigation has been carried out for three different converging angles such as 0°, 6.3°, and 12.7°. The stream wise distance of 30 mm has been maintained between two pin fins. The dimples/protrusion shave been placed 15 mm away between the pin fins. The circular pin fin diameter (d) has to be maintained at 10 mm. The hemispherical dimples/protrusions diameters have to be maintained at 10 mm. The dimple depth to dimple diameter ($\delta m/dm$) ratio and protrusion height to protrusion diameter ($\delta p/dp$) ratio has to be fixed at 0.2. The commercial software ANSYS CFX has been used for numerical simulation. The geometrical model and the meshing of the computational domain have been carried out by using an in-house code based on MATLAB software. The inlet and outlet segment has been considered adiabatic one. The end wall surface and pin fin surfaces have been supplied with a constant heat flux of 3280W/m². The end wall surface and pin fin surfaces are considered as no-slip boundary conditions. The temperature of the air at the inlet has to be maintained at 297.55K and the turbulence intensity has to be maintained at 5%. The governing equations such as continuity, momentum and energy have been used in numerical simulation. The wedge duct of larger converging angle incorporated with pin fins dimple provides better heat transfer rate due to the presence of phenomenon such as flow acceleration, increase of impingement zone and contraction of the flow recirculation zone inside the dimple. The large converging angled pin fin dimple wedge duct showed a higher friction factor. The larger converging angle Pin fin protrusion wedge duct produced a high heat transfer rate due to flow acceleration and more intense impingement on the protrusion. It also produced a large pressure loss penalty as per the area goodness factor (Nu/Nu0/f/f0) and volume goodness factor (Nu/Nu0/(f/f0)^(1/3)) the pin fin protrusion wedge duct with an angle of convergence 0° showed the best heat transfer performance. The wedged shape showed an enhancement of 2.1% for the area goodness factor and 4.5% for volume goodness factor as compared to the base line pin fin dimple (pin fin dimple duct with 0° converging angle). Sparrow et al. [51] studied numerically various sub regimes within the laminar flow regimes in a channel imprinted with hemispherical dimples and protrusions. The investigation has been carried out for the Reynolds number ranges 200 to 800. A parametric variation of Reynolds number based on the dimple/protrusion diameter was made covering the value 100,200 and 300. In terms of channel height, the Reynolds number values were 200,400,600 and 800. The hemispherical dimples/protrusions of diameter D and depth equal to D/2 have been imprinted on the lower as well as the upper wall of the channel, respectively. The dimple and protrusion have been offset by a distance equal to half of the pitch. The inter-plate

spacing, the height to diameter ratio have been maintained at H and H/D = 2, respectively. The pitch to diameter ratio has been maintained at 3. The governing equations such as the 3D Navier stoke equation and continuity equation has been used for the velocity fields. The commercial software CFX has been employed for numerical analysis. All of the residuals attained values of 10⁻⁶ and smaller for all of the investigated cases. At ReD (Reynolds number-based dimple diameter) = 100, small recirculation zones are present both upstream and downstream of the hemispherical blockage. The size of the recirculation zone upstream of the blockage is smaller than that downstream of the blockage. The smaller size in the recirculation zone, there is a minor role in creating pressure drop. At ReD = 200, the size of the recirculation zones has increased in size. The inertia losses are larger at ReD =200 compared to ReD = 100 due to the increase in the size of recirculation zones, but the friction losses are significant at ReD=200. At ReD = 400, the recirculation zones have greatly grown in size so that the upper part of the flow channel is completely engulfed by backflow due to such recirculation flow inertia-based pressure losses increased. The recirculation-based losses are known to be proportional to the square of velocity. It is observed that the laminar flow regimes included three sub regimes such as friction dominated flow, inertia loss dominated flow and transition between these flows. Xie et al. [52] investigated numerically heat transfer rate of a blade tip with internal hemispherical dimple. The investigation has been carried out in a two- pass channel with 180° turn and arrays of dimple depressed on the internal tip-cap. The dimples are imprinted in a staggered fashion. The heat transfer augmentations and pressure drop have been investigated at Reynolds number range 100, 000 to 600,000. The aspect ratio of two-pass channels of the rectangular cross-section has been maintained at 1.2. The commercial software FLUENT of version 6.3.26 has been used for numerical analysis. The geometry generation, import and mesh generation has been carried out using GAMBIT software of version 2.4.6. The 3D turbulent flow fields and temperature in two-pass channels with and without staggered array dimple array have been investigated using the k-ϵ turbulence model. The governing equations such as continuity, momentum and energy have been used for analysis. The pressure and velocity fields coupling have been carried out using SIMPLEC algorithm. The bottom wall intended with dimple has been supplied with constant heat flux. All walls other than the bottom wall have been presumed to be insulated. The no-slip boundary conditions have been employed to the entire wall of the channel. At the inlet, uniform velocity and temperature and at outlet outflow boundary conditions have been imposed. At the inlet, the intensity of turbulence has to be maintained at 5%. The velocity profiles are flat before sharp turn in both smooth and dimpled channel. When the flow enters the turn the flow acceleration starts near the inner wall region and the flow

deceleration starts near the outer wall region. When the coolant passed through the 180° turns of the two-pass channel area of impingement, separation and recirculation are created. Two circulating zones occurred at the first pass channel corner and second pass corner. When the fluid passed through the 180^0 turn, a centrifugal force arises from the curvature and pressure difference produced a pair of counter-rotating vortices in the turn. These vortices which are generated in turn are significantly strong, which causes transmission of cold fluid from the centre towards the outer flow. The dimples force the vortices towards the tip-wall due to which the turbulent mixing of cold and hot fluid increased. The dimple use is very effective in augmentation of heat transfer from the gas turbine blade tip due to the presence of turn induced impingement and dimple induced advection. The dimple tip channel's heat transfer enhancement rate is two times higher than the smooth tip channel. The dimpled tip channel's pressure loss penalty is 2–5% higher than the smooth tip channel. It has been reported that the increased rate of pressure loss penalty is much lower as compared to the increased rate of heat transfer. The decrease in dimple depth reduced the heat transfer enhancement rate slightly at high lower Reynolds number. The Nu number ratio (Nu/Nu0) decreased and the friction factor ratio (f/f0) increased with the increase in Reynolds number. The Reynolds analogy performance parameter ((Nu/Nu0)/(f/f0)) and heat transfer augmentation quantity ((Nu/Nu0)/(f/f0)$^{1/3}$) increased for dimpled tip channel. Minkimet al. [53] investigated the heat transfer enhancement rate and pressure loss characteristics of a cooling channel imprinted with inclined elliptical dimples. The channel aspect ratio of 3.0 and the hydraulic diameter of 22.5 mm have to be maintained. Total 14 numbers of dimples in seven rows have been arranged in inline fashion on the cooling channel. The investigation has been carried out by comparing the heat transfer rate of circular dimple imprinted cooling channel(reference) and inclined elliptical dimple imprinted cooling channel (optimum). The study has been carried out at Reynolds number range 10,000 based on hydraulic diameter. The flow fields and heat transfer analysis and 3-dimensional continuity, RANS (Reynolds Averaged Navier's stoke) and energy equations have been solved using a commercial code ANSYS CFX version 11.0. The unstructured grid pattern has been adopted for the simulation of the computational domain. Uniform velocity boundary condition at the inlet and constant pressure boundary condition at the outlet has been set. A constant heat flux value of 600 W/m² has been supplied to the dimpled wall cooling channel. No slip boundary conditions have been set for all walls. The low Reynolds number shear stress transport (SST) model has been employed as the turbulence closure. The lower heat transfer rate has occurred in the front part of both the dimple and approaches the peak value at rear rim. The flow separation at the front rims of the dimples caused a low heat transfer rate and the heat transfer rate enhanced

as the flow proceeds downstream due flow reattachment. The optimum inclined elliptical dimple showed a higher level of overall Nu number than the reference circular shape. The Nu number of elliptical shapes intended cooling channel is two times higher than the circular dimple imprinted cooling channel. The maximum heat transfer regions are found near the rear rim on the right of the flow direction. The heat transfer rate of inclined elliptical dimples has been enhanced by 81.2% as compared to circular dimples, whereas the pressure drop increased by 31.7%. Won et al. [54] studied the flow characteristics experimentally along and above the dimpled surface for three different relative dimple depths (δ/D) 0.1 to 0.3. Total 29 numbers of dimples are employed in a staggered fashion in stream wise direction with 4 to 5 dimples in each row. The different Reynolds number ranges are used for three different dimple depths. The dimple with deeper depth produced greater flow disturbance; hence for deeper dimple, the Reynolds number used is lower, whereas the shallow depth dimple provides less disturbance in the flow; hence for this case, a higher Reynolds number value is used. For all three dimple's depth, a primary vortex pair shedding at the central part of the dimples with the increase in dimple depth the primary vortex pair becomes more complex, more distorted and the edge vortex seems to be bigger. The magnitude of vortices increases as the Reynolds number increases for all three values of dimple depth. The highest magnitude of maximum vortices was produced in the deep dimple. The heat transfer augmentations are higher due to stronger vortices because the associated secondary flows are greater. There is also greater shear mixing, which increases three-dimensional turbulent transports. The primary vortex pair ejection frequencies range about 7–9 HZ and edge vortex pair oscillation frequencies range about 5–7 HZ for REH = 20,000 regarding dimple depth.

Rib generation by machining

The solar absorber plates are equipped with ribs, which are generated by machining. The experimental investigations are reported in the literature to study heat transfer rate and friction characteristics of rib incorporated solar absorber plate. In order to produce artificial roughness of different shapes, sizes and orientations ribs have been used on the absorber plate by this method as discussed in the following paragraph. The solar absorber plate incorporated with various roughened elements is shown in Figure 5 [9, 55–57].

Karwaet al. [9] investigated the performance of solar air heaters with chamfered repeated rib-roughness on the airflow side of the absorber plates experimentally. The roughened elements have a relative roughness pitch (P/e, where P is the pitch of the rib and e, is the height of the roughness) of 4.58 and 7.09 while the rib chamfer angle is fixed at 15°. The airflow duct depths of 21.8, 21.5 and 16 mm have been taken for investigation. The relative roughness heights (e/
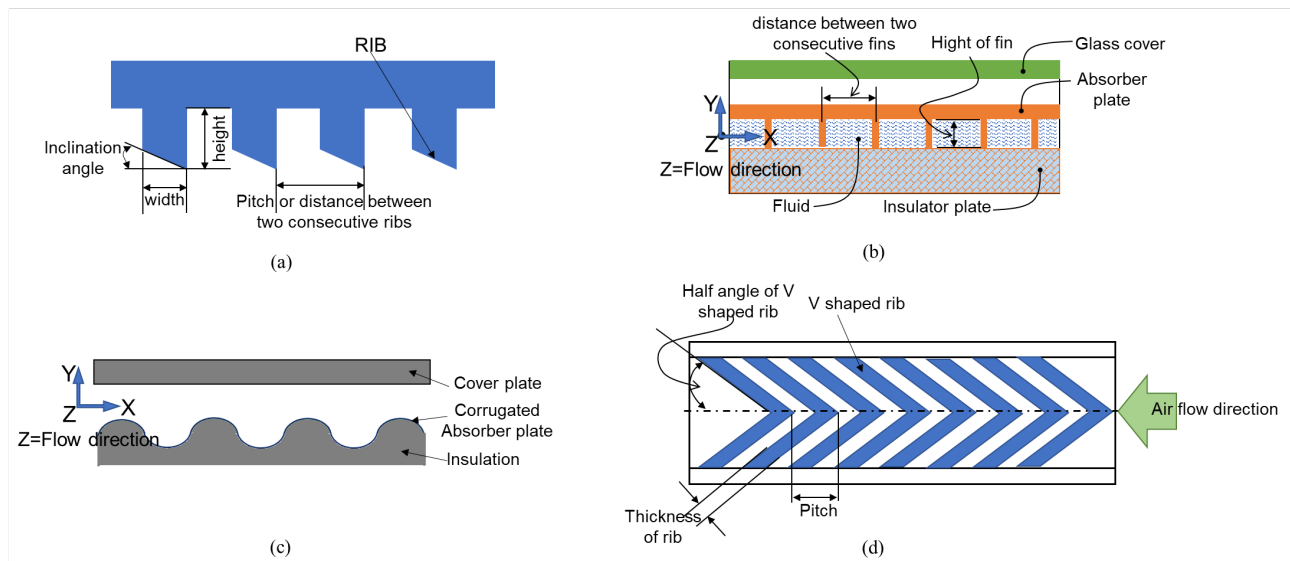
Figure 5. Solar absorber with various heat transfer enhancer, (a) Rib tarbulator solar absorber, (b) finned solar collector, (c) Corrugated solar absorber plate and (d) V shaped ribs solar absorber plate.

Dh where e is the roughness height and Dh is the hydraulic diameter of the duct) for the three roughened plates used are 0.0197, 0.0256 and 0.0441, respectively. The air flow rate per unit area of the absorber plate has been varied between 0.024 and 0.102 kg/s-m². The Reynolds number value will be varied from 3750 to 16350.

The roughened wall was uniformly heated, with the remaining three walls insulated. The thermal efficiency of solar air heaters with artificially roughened absorber plates increased by 10%to 40% compared to smooth surface absorber plates due to enhancement in the Nu number 50% to 120%. The pumping power requirement also increased due to the increase in friction factor 80% to 290%. It has been concluded that the enhancement of Nu number, friction factor and thermal efficiency wholly dependent on roughness element height. It has been observed that the solar air heater performance enhancement rate is higher at the highest relative roughness height. The effective efficiency at first increases with the increase in the Reynolds number attains a maximum value. However, it starts decreasing due to a substantial increase in the pumping power and it varies as the cube of the flow velocity. When the flow rate is lower and it is required to achieve the higher temperature of the air for application, the solar air heater must be incorporated with the roughness element of large relative roughness height. Higher pumping power is required at high flow rates. The gain in energy collection at greater relative roughness height is lower as compared to the pumping power required at high flow rates. As the pumping power required is higher than the energy gain at greater relative roughness height, the smaller roughness height is maintained to increase the energy collection rate. At a higher flow rate, the smooth channel provides better

effective efficiency. Momin et al. [57] studied the effect of the geometrical parameters of the V- shaped ribs on heat transfer and fluid flow characteristics of rectangular duct solar air heater whose absorber plate underside is incorporated with V-shaped ribs. The geometrical parameters such as relative roughness height e/Dh (where e is the roughness height and Dh is the hydraulic diameter of the rectangular height) of 0.02 to 0.034(the relative roughness height taken are 0.02, 0.022, 0.028 and 0.034) and angle of attack of 30° to 90° (angle of attack varies as 30°, 45°, 60° and 90°) for a fixed relative pitch of 10 have been for investigation of solar air heater performance. The investigation has been carried out at a Reynolds number range from 2500 to 18,000. The performance of the smooth duct solar air heater has been investigated for the same flow condition. The result of the V-shaped rib roughened duct solar air heater is compared with a smoother one. The Nu number increases, whereas the friction factors decrease with an increase of Reynolds number. The value of Nu number and friction factor is substantially higher as compared to the smooth absorber plates. This is due to the change in fluid flow characteristics as a result of roughness associated with absorber plate, which causes flow separations, reattachment and generation of secondary flow. The rate of enhancement of Nu number as compared to the friction factor with the increase in Reynolds is lower. This is due to the fact that the increase in relative roughness height the reattachment of free shear layer is not possible and the rate of heat transfer enhancement will not be proportional to that of friction factor. The maximum enhancement of Nu number and friction factor due to the presence of artificial roughened element has been found to be 2.30 and 2.83 times that of the smooth duct for an angle of attack 60°. The same value of angle of

attack provides maximum Nu number value and friction factor value. The thermohydraulic performance parameters improve by increasing the angle of attack of flow as well as by increasing relative roughness height. The maximum thermohydraulic performance has been obtained at an angle of attack 60°. It has been observed that at relative roughness height of 0.034, angle of attack of 60° and Reynolds number value of 17034 the v-shaped ribs solar air heater enhanced the Nu number by 1.14 times over inclined ribs whereas it is enhanced by 2.30 times then the smooth plate case. Karim et al. [58] studied the performance of three different types of solar collectors named as flat, finned and V-corrugated (60°) under different mass flow rate conditions. The performance of the three different solar air heater is investigated for the mass flow rate of 0.056 kg/m²s, 0.0387 kg/m²s, 0.0317 kg/m²s, 0.0248 kg/m²s and 0.0154 kg/m²s. The collectors are also investigated in double- pass mode to investigate the extent of improvement in efficiency that can be achieved without increasing the collector size or cost. During each test, the inlet temperature of air and flow rate remains constant from the experimentation data, it is evident that the flat plate collector with single pass is least efficient and the V-groove collector provides the highest efficiency. The V-groove collectors are also structurally stable. The V-corrugated collector has 7% to 12% higher efficiency than that flat plate collector and 5% to 9% more efficient than the finned collectors as shown in Figure 6 [58]. The V-corrugated collector can absorb a greater quantity of solar radiation compared to the flat plate and finned collectors of equal absorptivity. The absorption capacity of v-corrugated solar collector is higher because of multiple reflection and absorption of incident radiation. The efficiency of all three air collectors is a strong function of the mass flow rate of air. The efficiency is enhanced with flow

rates and tends to saturate beyond a flow rate of 0.056 kg/m²s because the outlet temperature of the air is decreased. The optimal ranges of flow rate suitable for drying of agricultural products are between 0.025 and 0.035 kg/m²s. Since the V-corrugated collector provides better efficiency in both the single and double pass operation and also structurally stable, this collector is considered predominantly useful for drying application.

Choudhuary et al. [56] studied the effects of air flow velocity and air channel depths on the air temperature increment, the collector efficiency and pressure drop experienced by the flowing air for different channel lengths and different specific mass flow rates of air. The studied have been carried out using two different type of solar air heater named as corrugated and plane solar air heater. The investigation is carried out for 5 different configurations. Type - 1 in which the absorber plate is corrugated and the cover plate is plane, Type - 2 the lower side of the cover plate is corrugated and absorber plate is plane, Type - 3 the cover plate as well as absorber plate is plane, Type - 4 the absorber plate is corrugated and the back plate is plane, Type - 5 the cover plate, absorber plate and back plate is plane. The Type - 1 configuration thermal performance has been higher as compared to others. When the mass flow rate increases the efficiency increases. The increment is rapid at low flow rate whereas increment in efficiency is less rapid at higher flow rates. The efficiency for a fixed collector length and specific air flow rate increases initially rapidly with the increase in air velocity and then increases slowly. The increment in efficiency with the increase in air velocity for a fixed collector length and flow rate increases in shallow depth air channel. The dependence of efficiency on air velocity is more predominant at higher mass flow rate then lower flow rate. The increment of flowing air temperature decreases the efficiency of the solar air heater. The efficiency of solar air heater at higher flow rate as well as lower flow rate and temperature rise of flowing air depends on the velocity of the air. The rise of temperature of the flowing air can be increased by decreasing the air flow rate per unit area and the loss in efficiency at lower flow rates can be avoided by increasing the channel depth for a fixed specific air flow rate and a fixed air velocity the system efficiency decreases with increase in the air channel depth. For fixed specific air channel length, the efficiency increases with increased air velocity or with decreased in air channel depth. With the increase in mass flow rate for a specific length of the collector, air velocity and with decrease in air channel depth the pressure drops increases. Kabeel et al. [59] investigated the thermal performance of flat, finned, and V-corrugated (60°) single glass cover, single-pass solar air heater experimentally. The influence of the mass flow rate of air on the exit temperature and thermal efficiency of the heater has been studied by taking three different values of mass flow rate such as 0.062, 0.028 and 0.009 kg/sec. The thermal efficiencies of the V-corrugated solar heater obtained at the
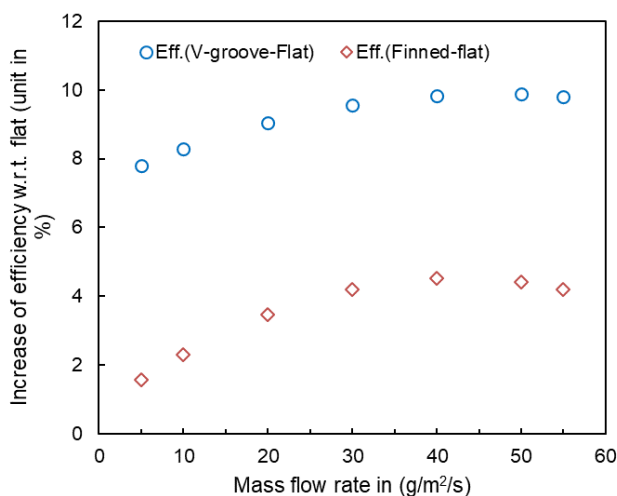
Figure 6. Variation of Efficiency with flow rate of solar air heater.

mass flow rate 0.062, 0.028, 0.009 kg/sec are 50%, 43.2% and 22.2%, respectively. For finned and flat solar heater thermal efficiencies obtained are 41.8%, 39.1%, 18.6% and 40.6%, 32%, 14.4% when the mass flow rate is 0.062, 0.028 and 0.009 kg/sec, respectively. The V-corrugated collector is found to be one of the most efficient collectors and the flat plate collector is one of the least efficient collectors. It has been concluded that the V-corrugated solar air heater shows thermal efficiency of about 8% to 14.5% and 6% to 10.5% higher than the flat plate and finned plate solar heater for mass flow rate 0.062 kg/s. The exit temperature of the v-corrugated solar air heater, which provides the best performance increases by 5°C when the mass flow rate is 0.062 kg/sec. The exit temperature of the v-corrugated solar air heater is 3.5°C more than the flat plate and finned plates when the mass flow rate is 0.062 kg/sec. The convection heat transfer coefficient of v-corrugated type solar air heater1.64 times higher than the flat type solar air heater and 1.36 then the finned type solar heater for the flow rate of 0.062 kg/sec. The V-corrugated solar air heater has a higher heat transfer area than the finned and flat surface solar air heater. It is clear from the Figure 7 [59], where the efficiency ratio of finned type to flat type is approximately unity. Hence thermal efficiency by finned type solar air heater is not significant as compared to v-corrugate. In addition, the maximum thermal efficiency obtained during noon time. The rise of air temperature with respect to flat type solar air heater, v-corrugated is more significant than finned type solar air heater (Figure 8) [59]. Like efficiency, the temperature rise also more during noon time. The turbulence inside the air channel increases due to which the collection of useful heat by the V- corrugated solar heater is higher than the finned and flat solar air heater.
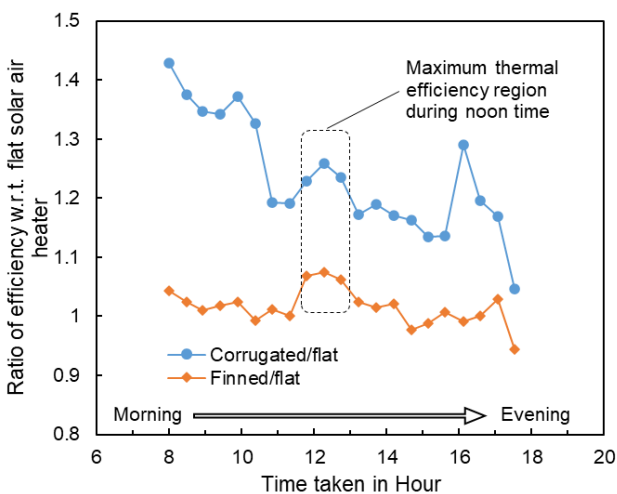
Wire fixation

Figure 7. A comparison of instantaneous thermal efficiency between V-corrugated /finned and flat plate solar air heater.
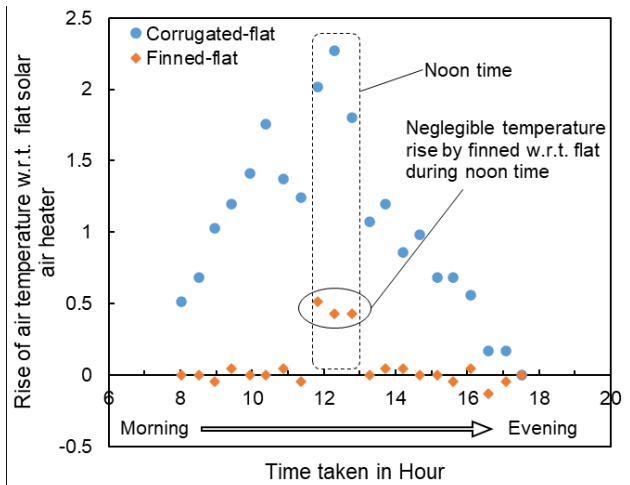

Figure 8. A comparison of measured temperature difference of air between V-corrugated/finned and flat plate solar air heater.

The heat transfer enhancement and friction loss characteristics of solar absorber plate have been studied by various investigators by fixing protruding wires of different shapes, size and orientations as an artificial roughness element on absorber plate.

Hachemi et al. [61] studied the enhancement of thermophysical properties of air, which is used as a fluid for heat transfer in solar air heaters using fins. The effect of fin dimension, as well as the distance between two consecutive fins on heat transfer rate, has also been studied. A fully developed flow has been created by soldering rectangular type fin under the absorber plate, arranged in a staggered fashion to enhance the heat transfer rate of air. Due to this arrangement, the fluid flow undergoes contraction followed by expansions, which creates a fully developed turbulent flow and increases the thermal heat transfer between the absorber plate and the air. The use of fin enhances the surface area for heat transfer, due to which there is an appreciable improvement of the thermal performance of solar air heaters as compared to those solar air heaters with plane absorber plate. The staggered arranged solar air heater efficiency increases as compared to the plane absorber plate. The heat transfer rate increases with the decrease in distance between the consecutive fins. The thermal heat performance for a specific mass flow rate 50 kg/h-m², length of the fin 10.0 cm and distance between the two consecutive staggered rows fin 2.5 cm is 38.6% for plane absorber plate and for finned absorber plate is 75.5% and the temperature rise increases for the plane absorber plate is 27.7°C and for finned absorber plate solar heater 54.1°C. Kabeel et al. [60] studied the effect of the shape factor of triangular type absorber plate solar air heater and longitudinal fins type solar air heater on collector efficiency. The flow passes over and under the absorber plate in the case of a triangular type solar air heater. Whereas the flow passes between the

absorber plate and first glass cover in case of longitudinal type solar air heater. The collector efficiency factor is a function of the absorber shape factor. The collector efficiency increases with the increase in the absorber shape factor. The increment rate of collector efficiency is higher up to the shape factor 3, and then the increment rate on further increasing shape factor is very low. The collector efficiency factor for the triangular type solar air heater is higher than the longitudinal fins type solar air heater. The heat transfer rate to the flow as well as the pressure loss penalty in the solar air heater increases with the increase of the triangular angle of the triangular collector. The optimum angle of the triangular collector varies from 50º to 60º.

Akpinar et al. [62] investigated the thermohydraulic performance of solar air heaters incorporated with 3 different types of obstacles. The obstacles incorporated into absorber plates are categorised as Type-I, Type-II, and Type-III and the solar air heater without obstacles is considered as Type-IV. Type-I obstacles are triangular obstacles of 5×5 cm^2 dimension, which are situated on the absorber plate at 10 cm intervals with 3.5 cm distance between the successive lines. Type-II obstacles are the leaf-shaped obstacles of 5 × 5 cm^2 dimension, which are situated on the absorber plate at 10 cm intervals with 3.5 cm distance between the successive lines. Type-III is the rectangular obstacles of (10 × 10) cm^2 dimensions, which are situated at 2.5 cm intervals at a 45º angle on the absorber plate. The investigation is carried out for two different mass flow rates of 0.0074 kg/sec and 0.0052 kg/sec. From the experimental data recorded, it is evident that the efficiency of the solar air collector depends significantly on the solar radiation, the surface geometry of the collector and the extension of the airflow lines. The intensity of solar insolation is highest at 12.30 PM. The highest daily solar radiation is obtained as 1016 W/m^2. The intensity of radiation increases in the morning to a peak value of 1016 W/m^2 at noon and starts decreases in the afternoon. The highest intensity of radiation is absorbed by Type-II type solar absorber plate and the lowest is Type-IV type solar absorber plate. The highest temperature increases occurred at periods of 12.00–14.00. The maximum difference temperature increase through the four types of solar air heaters (I-IV) was 45.9, 50.5.44.1 and 33.1ºC for 0.0074 kg/sec, 47.4, 55.4, 48.5 and 38.3 for 0.0052 kg/sec. The highest temperature difference increases occurred through Type-II, whereas the lowest enhancement through Type-IV. The efficiency of the collectors improves with increasing mass flow rates due to an enhancement of heat transfer to the airflow. The highest temperature difference enhanced efficiency and reduces the overall heat loss. From this, it is concluded that the obstacles ensure good airflow over and under the absorber plate, create turbulence and reduced the dead zones in the collector. Ong [63] theoretically studied the thermal performance of four different types of flat plate solar air heater and compared the result with the experimental result. The surface and air temperature have been

predicted theoretically at Reynolds number range from 3300 to 40,000 for four different solar collectors. The matrix inversion solution procedure to obtain a theoretical prediction of the performance has been used. The various types of solar air heaters used for the investigation were Type-IIa, Type-IIb, Type-III and Type-IV. Type-IIa solar collector was a single airflow between the absorber and bottom plates with no bottom insulations. Type-IIb was a single-channel design with a single airflow between the absorber and bottom plates with bottom insulation provided. Type-III was a double design with single airflow between absorber plates and with bottom insulation provided. Type-IV was a double channel design with double air flows between top glass and absorber and bottom plates and bottom insulation. It has been concluded from the study that temperature decreases with the increase in flow rates. The absorber plate exhibited the highest temperature with glass being at the lowest. The temperature difference between the air streams and the bottom plate becomes less with the increase in air flow rate. The result showed that the agreement between experimental data and predicted results was within 5°C. The type II obstacles provide a higher temperature difference as shown in Figure 9 [62].

Yeh et al. [64] investigated experimentally and theoretically the effect of the parallel barrier on collector efficiency and compared the collector efficiency of solar collectors without barrier. The collector efficiency has been investigated for three different mass flow rate 0.0214 kg/sec, 0.0161 kg/sec and 0.0107 kg/sec and for two different solar radiation intensity 1100 W/m^2 and 830 W/m^2. The barrier converted the solar collector into two sub-collector. The surface area of the solar collector has been maintained constant at 0.42135 m^2 (Where L (Length) = 26.5 cm, B
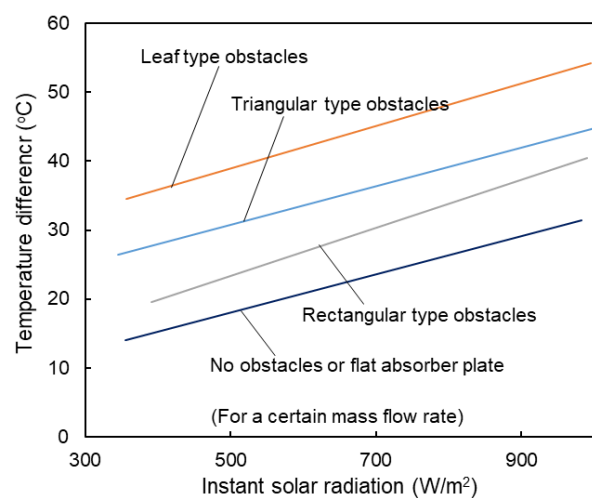

Figure 9. Variation of instantaneous solar radiation and temperature difference with time at different air flow rates (Type I: Triangular obstacle, Type II: Leaf shape obstacle, Type III: Rectangular obstacle and Type IV: No obstacle).

(width) = 159 cm), but the location of the barrier has been changed. The changes in the location of the barrier provided in nine different ratios of B1/B such as 1/6, 1/5, 1/4, 1/3, 1/2, 2/3, 3/4, 1/5 and 5/6. The barrier used to divide the flow channel was thin and thermally separated. The investigation concluded that with the increase in B1/B, the collector efficiency increased and it was maximum at B1/B = 0.5 and with the increase in B1/B further, it decreased. More parallel barriers placed inside the collector with the same distance between any two of them, the higher collector efficiency can be obtained by increasing either the aspect ratio (L/B) or barrier number, which decreases the cross-sectional area of the air duct and thus increases the velocity of airflow as well as the convection heat transfer rate from the surface of the absorbing plate to the flowing air. The collector efficiency is higher at a higher flow rate and it is maximum at B1/B = 0.5. The result showed an agreement between experimental and predicted results. Bhusan et al. [65] studied the heat transfer rate to the flowing air in the artificially roughened duct of the solar heater. They reported various roughness geometries such as chamfered ribs, dimple/protrusion, corrugated ribs, V-shaped ribs, and fins for studying heat transfer and friction characteristics of an artificially roughened duct of the solar air heater. It has been observed that artificial roughness is a good technique to improve a solar air heater's thermal performance. Leon et al. [66] studied the heat transfer rate numerically and flow resistance of both arrays of staggered and non-staggered rectangular fins. The investigation has been carried out for three different models such as standard, staggered A and staggered B model. In the standard model (none staggered) the thickness and length of the fin have been taken as 0.583 mm and 34.3 mm, respectively. In the staggered model and staggered model B the length of the fin has been split into two equal halves, each half of length 17.15 mm. The cooling fin area for standard and staggered model A has been maintained equal, whereas for staggered arranged model B it has been maintained a little bit smaller. The Reynoldsnumber with d as the characteristics length has been varied from 233.92 (u0 = 1.0 m/s and d = 3.417 mm) to a maximum value of 1403.54 (u0 = 6.0 m/s and d = 3.417 mm). The investigation has been carried out at the laminar flow regime. The numerical simulation has been carried out using computational fluid dynamics software FLUENT. The inlet velocity and temperature have been considered to be uniform. The walls of the cooling fins have been considered as smooth, impermeable and have no slip. The temperature at the wall of the cooling fins has been taken as uniform and constant. The governing equations such as continuity, momentum and energy have been used for numerical analysis. In this case, two types of grid patterns have been used one is coarse and the other is fine. The fine grid has been used to obtain heat flux and pressure drop. The staggered models have significant improvement in the total heat released, or it has higher overall performance due to regeneration of the boundary layer. Staggered model B is better as compared to model A. In staggered model B there is a significant improvement in heat transfer rate without a dramatic increase in pressure drop. For staggered model A the increase in heat transfer is higher but at the expense of a much larger increase in pressure drop. Staggered model B has less material due to its shorter length, which results in a significant economy. For equal heat transfer, the standard model incoming velocity of coolant fluid increased, whereas it decreased for staggered model B. At equal heat transfer, the pressure drop of the staggered model B is smaller. The quantity factor, which is the ratio between heat removed and consume power, increased significantly for staggered model B. The staggered model B with an incoming velocity of 4 m/s released 5.80% more heat than the standard model with 6 m/s and the staggered model B consumed 59.51% less power.

Pakdamann et al. [67] investigated experimentally the different thermal characteristics of natural convection solar air heater, which has been incorporated with a longitudinal fin array. From the investigation, it has been concluded that the heat transfer of the solar air heater can be enhanced by the attachment of longitudinal rectangular fins array. The heat transfer enhancement in the solar air heater is due to the increase in additional surface area as well as due to the mixing effect introduced by these elements. It has been observed that due to the increment of heat transfer surface area by 66% the increase in heat transfer rate is about 20%. The heat transfer rate is also a negligible dependency of the inclination angle of these devices. The thermal efficiency of finned incorporated solar air heater increases due to the increase in solar radiation intensity and the increase in ambient temperature. And its maximum value is obtained at noontime. It has been evident from experimental results that the effect of solar radiation intensity on the thermal performance of the system to be 79 times greater than the effect of the ambient temperature.

Solar thermal system with nanofluids

Two important factors are taken into consideration to produce an effective thermal collector. One is the selection of a suitable absorber plate and another one is the selection of suitable working fluid for efficient conversion of incident solar radiation into thermal energy. The use of appropriate working fluid helps to enhance the efficiency of solar collectors [4]. Nanofluids (solid-liquid composite material) are new kind of heat transfer fluid, which consists of small quantity of nano sized particles [68]. These nano particles are suspended uniformly and stably in different type of base fluid [68]. The pure metals (Au, Ag, Cu, Fe), metal oxide (CuO, SiO_2, AlO_3, TiO_2, ZnO, Fe_3O_4), carbides (SiC, TiC), Nitrides (AlN, SiN) and different type of carbons (diamond, graphite, single/multi wall carbon tubes) can be used as nanoparticles [69]. The liquid such as water, glycol, ethylene and engine oil can be used as base fluid [69]. Nanofluids have the tendency to provide higher efficiency

due to their outstanding optical and thermophysical properties. Nanofluid does not block the flow channel as well as there is very less pressure drop during the flow [68]. Hence Nanofluid can be considered as future heat transfer fluid in many heat transfer applications [68].

Abdelrazik et al. [4] studied the optical potential of water/M Xene nanofluid by varying the M Xene concentration from 0.0005 to 0.05 wt% and using two different types of surfactant named as CTAB or SDBS in a hybrid PV/T system. From the investigation, the M Xene concentration and the types of surfactant used to play a vital role in transmittance, absorbance and dispersion stability of the water/M Xene nanofluids. It has been concluded from the investigation that; (i) the nanofluid prepared by using CTAB surfactant is more stable when the concentration of nanoflakes are higher, (ii) the nanofluid prepared by using SDBS surfactant are more stable when the concentration of nanoflakes are low, (iii) the transmittance rate decreases when the concentration of nanoflakes increases, (iv) the effect of surfactant and concentration of nanoflakes is noticeable when the wavelength is 300–1350 nm, (v) the water/M Xene nanofluid prepared using SDBS surfactant has higher transmittance as compared to the nanofluid prepared by using CTAB surfactant, (vi) the performance of the hybrid PV/T system is higher as compared to the conventional PV/T system when the low concentration water/M Xene nanofluid is used, (vii) when the concentration of M Xene is above 0.05 wt% the hybrid system with optical filtration becomes electrically in efficient.

Krishna et al. [5] studied and compared the various types of nano heat transfer enhanced fluid used in parabolic trough solar collector. From the investigation, it has been observed that the parabolic trough solar collector use is significant as compared to other concentrated types of solar collector as the operating temperature range varies from 150°C to 800°C. As the operating temperature range of the parabolic trough collector is high, so it can be used for power generation. It has been concluded that the conventional fluid which is used for heat transfer in parabolic trough collector has poor heat transfer ability and less capable in the conversion of solar energy into thermal energy. The solution to this type of problem as well as the enhancement of overall efficiency of the system, has been obtained either by enhancing the thermophysical properties of the heat transfer fluid or by using nano-enhanced heat transfer fluid. So, in comprehensive literature review enhancement of thermophysical properties of molten salts by doping nanoparticles and their enhancement in thermal stability at high temperature, the possibility of using mono and hybrid nanofluid, ionic liquids, gaseous heat transfer fluid and vegetable oil as heat transfer fluid in parabolic trough collectors have been discussed. The important point which has been obtained from the literature review on heat transfer fluid used for parabolic trough solar collector are as follows; (i) heat transfer must have low melting point, (ii) stable at high temperature, (iii) high specific heat, (iv) high thermal conductivity, (v) low corrosion rate, (vi) low dynamic viscosity, (vii) low cost, (ix) low toxicity flammability, (x) low explosivity (xi) to increase the thermal efficiency the heat transfer fluid with higher latent heat capacity must be used, (xii) addition of nano particle like CuO, CNT, MWCNT to heat transfer fluid to modify the thermal properties.

The reported nanofluids are preferable for the solar thermal system such as a solar water heater. It also has many industrial applications such as nuclear reactors, the transportation industry, electrical energy, solar absorption and bio-medical fields [69]. The nanofluid has good solar radiation absorption properties and high thermal conductivity so nanofluids can be used in the solar thermal system to enhance its performance [69].

DISCUSSION

The heat transfer rate of spherical concavities intended surface enhanced by 30%–40% than the smooth surface as there is no brake away around such relief [17]. The teardrop shape concavities intended surface have a high heat transfer rate as compared to the spherical cavity. The overall heat transfer rate of both the concavities is 2.5 times that of the smoother counterpart for the Reynolds number range $10,000 \leq Re \leq 50,000$ [2]. The heat transfer enhancement of hemispherical concavities intended channel is constant and it is 2.1 time than the smooth surface channel when the H/D ratio varies from 0.37 to 1.49 in a thermally developed flow region. The friction factor of concavity intended surface for the aerodynamically fully developed region is around 0.0412 and it is 1.6 to 2.0 times than the smoother counterpart. The thermal performance of the dimpled surface is higher than the smoother surface. The thermal performance of the dimpled surface is equal to 1.75, whereas the thermal performance of the conventional rib lies between 1.16 and 1.60 [18]. For in-line dimple arrangement, the maximum Nusselt number is 25% higher as compared to the smooth surface [19]. The local and spatially averaged Nusselt number increases with the decreases in the ratio of inlet air stagnation temperature to surface temperature. This is due to the transmission of vortical fluid by cool fluid in the central region of the channel closer to the heated dimple surface [20]. The heat transfer enhancement rate of dimpled surface internal passages is about factor 2 or more than it if the relative dimple depth is 0.3 or higher than it and the surface area densities are equalto0.5 or higher than it [21]. It is reported that for the staggered arrangement, the maximum Nusselt number is 26% higher as compared to the smoother one. For in-line arrangement, the maximum Nusselt number is 25% higher than the smooth surface [22]. The Nusselt number and friction factor of the teardrop dimple increases with the increases of dimple depth and radius but decreases with the decrease in pitch. The enhanced tube with teardrop dimple with D =

2 mm, P = 15 mm, R = 4 mm and Re = 5000 showed largest performance evaluation criterion value about 2.06 [23]. The presence of only a single primary circulation zone in a triangular type dimple gives less heat transfer enhancement rate. The highest heat transfer augmentations and most significant local and the overall increase in eddy diffusivity for momentum and heat occur in spherical and tilted cylinder concavities [13]. A maximum reduction of 3.7K was observed in the oval dimple-2 vortical configuration showing potential benefits of dimples in laminar channel flow [24]. At Reynolds number of 1000, the performance level of the double protrusion wall is about 6.5 and the double dimple wall is about 6. The pressure drop of the double protrusion wall is higher due to a decrease in the cross-sectional area of flow [12]. The heat transfer augmentation up to 6% as compared to the flat plate consistently observed on both circular and oval dimple when the Reynolds number varies from 500 to 1000 [25]. The net result is an increased ratio of Nusselt number for the flat surface just downstream of the deeper dimples as δ/D increase. The friction factor increases with the increase in δ/D value [26]. The optimum number of fins required to get the best heat transfer behavior in dimple fins and the plain finsheat sink is 989 and 878. For in-line arrangement, the optimum numbers of fins required to get best transfer behaviour by dimple fin heat sink are 999 and for plain fin heat sink is 888, respectively [27]. The Overall Nusselt number augmentation as compared to the smooth laminar channel is about 2.94. However, at ReH = 9300 the dimpled surface contributes a higher pressure drop and it comes in the form of drag. The overall form drags increases from 44% at ReH = 220 to 80% at ReH = 9300. The overall form drag of dimples predominates over the protrusions. The overall friction co-efficient augmentation rate at lower Reynolds number value ranges from 1.67 to a high value at the highest Reynolds number [28]. It is observed that the overall Nusselt number increases with the increase of Reynolds number for lower channel height cases. With the decrease in channel height to dimple diameter ratio, the disturbance in the flow increases by the dimple, which causes a higher Nusselt number [29]. The heat transfer enhancement rate for deep concavities is about 2.5 times and for shallow indentation, it is about 2 times than the smooth counterpart [30]. Intensive mass transport by the heat transfer agent from the near-wall region to the outer region reduces the thermal resistance in the heating surface with the decrease in boundary layer thickness. Hence the convective heat transfer increases [31]. From Numerical simulation, it is found that the flow enters into the concavity forms two vortical structures. The vortical structure comes out from the cavity in two different ways. One vortical structure from the downstream cavity centre emerges out as a single bundle tube and another will emerge out from the concavity in a zigzag fashion separately. These flow features have significant effects on enhancing surface transfer [1]. The microchannel heat sinks with impinging jet having convex dimple exhibited the best cooling performance and provided less flow resistance in MIJS. Among all the dimples MIJ, the convex dimple provides the best overall performance, followed by MIJS without dimple, mixed dimple, and concave dimples [32]. The normalised Nusselt number values (Nu/Nu0) generally vary from 2 to1.2 inside the dimple. The lower values Nu/Nu0 are obtained along the upstream portion of the dimple floor and in the upstream, the value varies from 0.4 to 1. The higher value of Nu/Nu0 is obtained in the downstream portion of the dimple bottom (values in the range 1–3) [33]. Relative Nusselt number ratio (Nudimple/Nusmooth) increases for all dimple configuration to the levels 2.8–5.9 and 2.5–1.5 for laminar and turbulent flow, respectively. When 900 ≤ Re ≤ 30,000, the pressure drops penalties increase to the levels of 2 to 6.7 and 2.5 to 3.6 for laminar and turbulent flow conditions in dimple intended hexagonal duct. The area-averaged Nusselt number will follow the order convex- convex > concave-convex (convex) > concave-convex (concave) > concave-concave. The convex-convex dimple incorporated hexagonal duct's overall performance is higher compared to other [14]. The averaged Nu number of the double dimples and large dimples are on the same levels and are around 25% higher than that of the small dimple. The friction factor is decreasing with the increase in Reynolds number [34]. The pin fin dimple channel with δ/D = 0.2 and 0.3 produced Nusselt number values of about 8% and 19% to 14%, respectively. The Nusselt number values of the pin fin dimple channel are higher than that pin fin channel when the Reynolds ranging from 8200 to 50,500. The pin fin and pin fin dimple channel's overall thermal performance parameters reduce with the Reynolds number. At δ/D = 0.3 and 0.2 the overall thermal performance increased by 14.9% to 12.7% times higher than the pin fin channel, respectively [35]. The teardrop dimples showed the highest thermal performance of about 1.8. The thermal performance of teardrop dimples is about 11% higher as compared to the spherical shape dimples. The thermal performance obtained for inclined elliptical dimple has been approximately same as the spherical dimple. The elliptical dimples showed lower thermal performance and about 16% to 10% lower than the spherical dimples [16]. The averaged heat transfer augmentation of a spherical dimple showed 1.5 to 1.7 times and friction factor 1.2 to 2.0 times than the fully developed turbulent flow in a smooth circular duct. The teardrop dimples showed the heat transfer enhancement of 1.8 to 2.0 times and friction factor of 1.6 to 2.3 times, then the fully developed flow in a smooth circular duct. The teardrop dimple heat transfer enhancement and friction factor 18% and 35% to 15% higher than the spherical dimple. Due to the enlargement of the heat transfer surface area, the heat transfer rate of teardrop dimple was about 1.64 to 1.85 and spherical 2.0 to 2.2 times, then the fully developed smooth circular duct [36]. The ratio of Nu number decreased when e/Dh varied from 0 to 0.1 and it increased when it is larger than 0.1 for

teardrop dimple. The ratio of friction factor decreased with Reynolds when e/Dh < 0.2 and it has not changed much where Dh = 0.2 and decreased when e/Dh > 0.2. Thermal performance increased gradually as the centre moves downwards for the teardrop protrusion. The thermal performance value showed minimum value when e/Dh = 0.1 and increased as e/Dh > 0.1 for teardrop dimple. The thermal performance showed the maximum value for teardrop dimple and protrusion when e/Dh = 0.4[37]. As the Reynolds number within the channel increases, the thermal performance also increases. Relative to V-ribs, the V- dimple channel produced less loss of pressure [15]. The Nusselt number ratio of supercritical carbon dioxide is 2.3 times higher than air at Re = 90,000. The friction factor ratio is close to the air at Re = 90,000. The comprehensive thermal performance of supercritical carbon dioxide is 2.4 times than the air at Re = 90,000 [38]. The maximum Nusselt number value has been obtained at relative roughness height (e/D) 0.0379 and at relative pitch (P/e) 10. The minimum value of the friction factor has been obtained at relative roughness height (e/D) 0.02989 and at relative pitch (P/e) 10[39]. At a high flow rate, the smooth duct air heater has better effective efficiency [3]. The maximum enhancement of Nu number and friction factor in an artificially roughened solar air heater has been found to be 2.30 and 2.83 times that of the smooth duct for an angle of attack 600. It is found out that for a relative roughness height of 0.034, angle of attack of 600 and Reynolds number of 17034, the V-shaped ribs solar collector enhanced the Nusselt number by 1.14 and 2.30 times over inclined ribs and smooth plate case [9]. The collectors' efficiency improves with increasing mass flow rates due to an enhancement of heat transfer to the airflow. The highest temperature difference enhanced efficiency and reduces overall heat loss [57]. The efficiency increases with increased air velocity or by decreasing in air channel depth for fixed specific air channel length. With the increase in the mass flow rate for a specific length of the collector, air velocity and decreased air channel depth, the pressure drop increases [58]. The V-corrugated solar air heater has a higher heat transfer area than the finned and flat surface solar air heater. The turbulence inside the air channel increases due to which the collection of useful heat by the v- corrugated solar heater is higher than the other two designs [56]. The staggered arranged solar air heater efficiency increases as compared to the plane absorber plate. With the decrease in distance between the consecutive fins, the heat transfer rate increases [59]. The collector efficiency factor for the triangular solar air heater is higher than the longitudinal fins solar air heater [61]. The efficiency of the collectors improves with increasing mass flow rates due to an enhancement of heat transfer to the airflow. The highest temperature difference enhanced efficiency and reduced the overall heat loss [60]. It has been concluded from the study that temperature decreases with the increase in flow rates [62]. The collector efficiency is higher at a higher flow rate and it is maximum at B1/B = 0.5[63]. It has been observed that artificial roughness is a good technique to improve the thermal performance of a solar air heater [64]. At the downstream of the hemispherical cavity, the average heat transfer increased as compared to the channel without cavity [65].

LIMITATIONS OF VARIOUS ARTIFICIAL ROUGHNESSES

From the investigation, it has been observed that the protruded artificial roughness like ribs, fins and baffles has been attached on gas turbine blade of the power plant, combustion liner, biomedical devices and solar thermal system to increase the heat transfer rate. Despite heat transfer enhancement, these protruded roughened elements have the following limitations and drawbacks;

a) Huge pressure loss- Due to the addition of these roughened elements, the friction between the flowing air and roughened surface increases, which creates excessive pressure loss.

b) High power consumption-The pressure penalty causes higher power consumption as high power is required to force the air to flow through the channel.

c) Uneven cooling- The pressure loss causes flow separation and this creates uneven cooling on the heat transferring surface.

d) Thermal stress development- Flow separation causes uneven cooling. Hence there is a possibility of the development of thermal stress.

e) Reduce longevity of component- The uneven cooling of components and development reduces the life span of the component.

f) Add extra weight – The attachment of excessive material on the heat transferring surface increases the extra weight to the system so that the system gets bulky, which is undesirable.

g) The generation of artificial roughness is a complex phenomenon and it may not be feasible for large scale production.

h) It needs higher maintenance cost.

Besides, geometry intended roughened surface is also used to enhance the heat transfer in various thermal systems. However, these roughened surfaces have some limitations and benefits compared to the protruded roughened surface.

a) Spherical, triangular dimple have higher inferior heat transfer area whereas teardrop has less inferior heat transfer area.

b) In teardrop dimple in the upstream half the slope present is straight due to which the flow separation and recirculation are less as compared to the spherical dimples.

c) In a Triangular dimple, only a single vortex is generated, which one of the main important phenomena to enhance the heat transfer rate.
d) The concavities are easily manufactured.
e) It requires less maintenance cost.

Findings with future recommendations

The heat transfer enhancement rate is less than the friction penalty in the case of the protruding incorporated flow channel. Whereas the heat transfers enhancement rate of dimple imprinted flow channel is higher as compared to the friction penalty. Among the various types of dimples intended flow channels, the teardrop imprinted flow channel has a higher heat transfer rate and thermal performance factor. As our aim is to develop new green technologies, reduce emissions, reduce consumption of non-renewable energy as well as focus on the use of renewable energy. In addition, it is necessary to reduce the weight of the system. Therefore, this type of concavity can be used in other thermal systems like solar air heaters and solar water heaters. More studies need to be carried out using this dimple in the solar thermal system in that direction. The study may include the analysis of geometry, the arrangement of the dimple and thermal performance factor in solar thermal systems experimentally and numerically.

CONCLUSIONS

In this present paper, an attempt has been made to report heat transfer and friction characteristics of protruded and indented roughened elements flow channels. Experimental and numerical studies carried out by various investigators have been discussed and reported in detail. Artificial roughness is a good technique to improve the thermal performance of the flow channel. It has been found out that artificial roughness such as protruded elements has a higher pressure penalty as compared to all types of concavities. Among all the concavities, the teardrop shape dimple roughness shape has the highest thermal performance. Solar air heaters and solar water heaters can be incorporated with a dimple to enhance the heat transfer rate. Compared to the spherical dimple, the inclined teardrop dimple has lower flow separation due to a slight loop structure in the initial half of the dimple, and thus the inclined teardrop dimpled channel shows higher heat transfer enhancement compared to the spherical dimpled channel. The inclined tear drop heat sink thermal performance was 7.36% higher as compared to the spherical dimple heat sink. The thermal performance of the heat sink can be significantly improved by employing spherical dimple and inclined teardrop dimple on the fin surface. The daily efficiencies of flat plate and spherical dimple plate solar air heater increase with the increasing mass flow rate of air. The heat transfer enhancement can be improved by enhancing fluid properties. The nanofluid has a higher solar radiation absorption capacity

and higher thermal conductivity. Nanofluid integrated with the roughened surface may be used to enhance the heat transfer performance in the solar thermal system.

NOMENCLATURE

H/D	Channel height to dimple imprint diameter. S/D = Relative pitch
δ/D	Dimple depth ratio
P	Pitch
D	Dimple diameter
R	Radius of dimple
S_T	Distance between centre of adjacent dimple in transverse direction
S_L	Distance between centre of adjacent dimple in stream wise direction
Re	Reynolds number
L/B	Aspect ratio
h_d	Dimple height
h_p	Protrusion height
D_h	Hydraulic diameter. Re_{Dh} = Reynolds number at Hydraulic diameter of channel
Nu	Nusselt number of dimple intended channel. Nu_0 = Nusselt number of smooth channel
D	Dimple
B	Bump
X/D	Stream wise spacing to diameter ratio
H/D	Fin height to diameter ratio
e/D_h	Relative roughness height
P/e	Relative roughness pitch
$P.F$	Performance ratio
δ_p/D_p	Relative dimple depth ratio for protrusion
D_j	Diameter of jet nozzle
e	Eccentricities
E/H	where E is the eccentricity between jet centre and dimple centre and H = jet-to-jet space
S/D_j	where S is the separation distance between the dimple surface to jet surface and Dj is diameter of jet nozzle
$((Nu/Nu_0)/(f/f_0))$	Reynolds analogy performance parameter
$((Nu/Nu_0)/(f/f_0)_{1/3})$	Heat transfer augmentation quantity

REFERENCES

[1] Lin Y, Shih TI, Chyu MK. Computations of Flow and Heat Transfer in a Channel with Rows of Hemispherical Cavities. Int. Gas Turbine Aeroengine Congr. Exhib. Gas Turbine Aeroengine Congr. Exhib. Indianap., 1999, p. V003T01A081. https://doi.org/https://doi.org/10.1115/99-GT-263.

[2] Chyu MK, Yu Y, Ding H, Beach WP. Concavity enhanced heat transfer in an internal cooling passage. 99-GT-263, 1999, p. 1–7.

[3] Schukin A V, Kozlov AP, Agachev RS. Calibrating Tests in Non-Gradient Flow in Conditions 1995.

[4] Abdelrazik AS, Tan KH, Aslfattahi N, Arifutzzaman A, Saidur R, Al-Sulaiman FA. Optical, stability and energy performance of water-based MXene nanofluids in hybrid PV/thermal solar systems. Sol Energy 2020;204:32–47. https://doi.org/10.1016/j.solener.2020.04.063.

[5] Krishna Y, Faizal M, Saidur R, Ng KC, Aslfattahi N. State-of-the-art heat transfer fluids for parabolic trough collector. Int J Heat Mass Transf 2020;152. https://doi.org/10.1016/j.ijheatmasstransfer.2020.119541.

[6] Aslfattahi N, Saidur R, Arifutzzaman A, Sadri R, Bimbo N, Sabri MFM, et al. Experimental investigation of energy storage properties and thermal conductivity of a novel organic phase change material/MXene as A new class of nanocomposites. J Energy Storage 2020;27:101115. https://doi.org/10.1016/j.est.2019.101115.

[7] Aslfattahi N, Saidur R, Sidik NAC, Sabri MFM, Zahir MH. Experimental assessment of a novel eutectic binary molten salt-based hexagonal boron nitride nanocomposite as a promising PCM with enhanced specific heat capacity. J Adv Res Fluid Mech Therm Sci 2020;68:73–85. https://doi.org/10.37934/ARFMTS.68.1.7385.

[8] Saxena A, Varun, El-Sebaii AA. A thermodynamic review of solar air heaters. Renew Sustain Energy Rev 2015;43:863–90. https://doi.org/10.1016/j.rser.2014.11.059.

[9] Karwa R, Solanki SC, Saini JS. Thermo-hydraulic performance of solar air heaters having integral chamfered rib roughness on absorber plates. Energy 2001;26:161–76. https://doi.org/10.1016/S0360-5442(00)00062-1.

[10] Mironov A, Isaev S, Skrypnik A, Popov I. Numerical and physical simulation of heat transfer enhancement using oval dimple vortex generators —Review and recommendations. Energies 2020;13. https://doi.org/10.3390/en13205243.

[11] Rashidi S, Hormozi F, Sundén B, Mahian O. Energy saving in thermal energy systems using dimpled surface technology – A review on mechanisms and applications. Appl Energy 2019;250:1491–547. https://doi.org/10.1016/j.apenergy.2019.04.168.

[12] Hwang SD, Kwon HG, Cho HH. Heat transfer with dimple/protrusion arrays in a rectangular duct with a low Reynolds number range. Int J Heat Fluid Flow 2008;29:916–26. https://doi.org/10.1016/j.ijheatfluidflow.2008.01.004.

[13] Park J, Ligrani PM. Numerical predictions of heat transfer and fluid flow characteristics for seven different dimpled surfaces in a channel. Numer Heat Transf Part A Appl 2005;47:209–32. https://doi.org/10.1080/10407780590886304.

[14] Chang SW, Chiang KF, Chou TC. Heat transfer and pressure drop in hexagonal ducts with surface dimples. Exp Therm Fluid Sci 2010;34:1172–81. https://doi.org/10.1016/j.expthermflusci.2010.04.006.

[15] Jordan CN, Wright LM. Heat Transfer Enhancement in a Rectangular (AR = 3:1) Channel With V-Shaped Dimples. Vol 5 Heat Transf Parts A B 2011;135:1505–16. https://doi.org/10.1115/GT2011-46128.

[16] Rao Y, Feng Y, Li B, Weigand B. Experimental and Numerical Study of Heat Transfer and Flow Friction in Channels With Dimples of Different Shapes. J Heat Transfer 2015;137:031901. https://doi.org/10.1115/1.4029036.

[17] Afanasyev VN, Chudnovsky YP, Leontiev AI, Roganov PS. Turbulent flow friction and heat transfer characteristics for spherical cavities on a flat plate. Exp Therm Fluid Sci 1993;7:1–8. https://doi.org/10.1016/0894-1777(93)90075-T.

[18] Moon HK, O'Connell T, Glezer B. Channel Height Effect on Heat Transfer and Friction in a Dimpled Passage. J Eng Gas Turbines Power 2002;122:307. https://doi.org/10.1115/1.483208.

[19] Mahmood GI, Hill ML, Nelson DL, Ligrani PM, Moon H-K, Glezer B. Local Heat Transfer and Flow Structure on and Above a Dimpled Surface in a Channel. J Turbomach 2002;123:115. https://doi.org/10.1115/1.1333694.

[20] Ligrani PM, Harrison JL, Mahmmod GI, Hill ML. Flow structure due to dimple depressions on a channel surface. Phys Fluids 2001;13:3442–51. https://doi.org/10.1063/1.1404139.

[21] Bunker RS, Donnellan KF. Heat Transfer and Friction Factors for Flows Inside Circular Tubes With Concavity Surfaces. J Turbomach 2003;125:665. https://doi.org/10.1115/1.1622713.

[22] Katkhaw N, Vorayos N, Kiatsiriroat T, Bunturat D, Nuntaphan A. Heat transfer behavior of flat plate having spherical dimpled surfaces. Case Stud Therm Eng 2014;Vol.2:67–74.

[23] Xie S, Liang Z, Zhang J, Zhang L, Wang Y, Ding H. Numerical investigation on flow and heat transfer in dimpled tube with teardrop dimples. Int J Heat Mass Transf 2019;131:713–23. https://doi.org/10.1016/j.ijheatmasstransfer.2018.11.112.

[24] Silva C, Park D, Marotta E (Ed), Fletcher L (Skip). Optimization of Fin Performance in a Laminar Channel Flow Through Dimpled Surfaces. J Heat Transfer 2009;131:021702. https://doi.org/10.1115/1.2994712.

[25] Park D, Silva CA, Marotta E, Fletcher L. Study of Laminar Forced Convection Heat Transfer for Dimpled Heat Sinks. J Thermophys Heat Transf 2008;22:262–70. https://doi.org/10.2514/1.33497.

[26] Burgess NK, Ligrani PM. Effects Of Dimple Depth on Channel Nusselt Numbers and Friction

Factors. J Heat Transfer 2005;127:839. https://doi.org/10.1115/1.1994880.

[27] Small E, Sadeghipour SM, Asheghi M. Heat Sinks With Enhanced Heat Transfer Capability for Electronic Cooling Applications. J Electron Packag 2006;128:285. https://doi.org/10.1115/1.2229230.

[28] Elyyan MA, Tafti DK. Large Eddy Simulation Investigation of Flow and Heat Transfer in a Channel With Dimples and Protrusions. J Turbomach 2008;130:041016. https://doi.org/10.1115/1.2812412.

[29] Shin S, Lee KS, Park SD, Kwak JS. Measurement of the heat transfer coefficient in the dimpled channel: Effects of dimple arrangement and channel height. J Mech Sci Technol 2009;23:624–30. https://doi.org/10.1007/s12206-008-1211-1.

[30] Belen'kiy, M.Y., Gotovskiy, M.A., Lekakh, B.M., Fokin, B.S., and Dolgushin KS. Heat Transfer Agumentation Using Surfaces Formed by a System of Spherical Cavities. Heat Transf Reasearch 1993;25:196–203.

[31] Chushkin, Yu. V., Kiknadze, G, I., and Kolyaskin OE. ThinWalled Shell of a Nuclear Reactor Fuel Element. Certif. No.1538190,IB USSR, 1990.

[32] X.Huang, W.yang,T.Ming, W.Shen XY. Heat transfer enhancement On a microchannel heat sink. Heat Mass Transf 2017;112:113–24.

[33] Zhou F, Acharya S. Experimental and Computational Study of Heat/Mass Transfer and Flow Structure for Four Dimple Shapes in a Square Internal Passage. Proc. ASME TurboExpo 2009Power Land, Sea Air, Orlando,Florida,USA: 2009, p. 1–15.

[34] Slabaugh CD, Tran L V., Kapa JS. Heat Transfer in a Rectangular Channel with Dimples Applied to One Wall. J Propuls Power 2012;27:1303–14. https://doi.org/10.2514/1.56285.

[35] Rao Y, Xu Y, Wan C. A Numerical Study of the Flow and Heat Transfer in the Pin Fin-Dimple Channels With Various Dimple Depths. J Heat Transfer 2012;134:071902. https://doi.org/10.1115/1.4006098.

[36] Rao Y, Li B, Feng Y. Heat transfer of turbulent flow over surfaces with spherical dimples and teardrop dimples. Exp Therm Fluid Sci 2015;61:201–9. https://doi.org/10.1016/j.expthermflusci.2014.10.030.

[37] Xie Y, Qu H, Zhang D. Numerical investigation of flow and heat transfer in rectangular channel with teardrop dimple/protrusion. Int J Heat Mass Transf 2015;84:486–96. https://doi.org/10.1016/j.ijheatmasstransfer.2015.01.055.

[38] Jing Q, Du Q, Xiong L, Zhang D. Numerical Predictions of Heat Transfer Performance in Dimple/Protrusion Channels with the Working Fluid of Supercritical Carbon Dioxide at High Re 2015:1–4. https://doi.org/10.2991/icectt-15.2015.5.

[39] Saini RP, Verma J. Heat transfer and friction factor correlations for a duct having dimple-shape artificial roughness for solar air heaters. Energy 2008;33:1277–87. https://doi.org/10.1016/j.energy.2008.02.017.

[40] Mahmood GI, Sabbagh MZ, Ligrani PM. Heat Transfer in a Channel with Dimples and Protrusions on Opposite Walls. J Thermophys Heat Transf 2001;15:275–83. https://doi.org/10.2514/2.6623.

[41] Mahmood GI, Ligrani PM. Heat transfer in a dimpled channel: Combined influences of aspect ratio, temperature ratio, Reynolds number, and flow structure. Int J Heat Mass Transf 2002;45:2011–20. https://doi.org/10.1016/S0017-9310(01)00314-3.

[42] Park J, Desam PR, Ligrani PM. Numerical predictions of flow structure above a dimpled surface in a channel. Numer Heat Transf Part A Appl 2004;45:1–20. https://doi.org/10.1080/1040778049026740.

[43] Perwez A, Kumar R. Heat transfer performance investigation of the spherical dimple heat sink and inclined teardrop dimple heat sink. Numer Heat Transf Part A Appl 2019;76:73–86. https://doi.org/10.1080/10407782.2019.1612676.

[44] Silva C, Marotta E, Fletcher L. Flow structure and enhanced heat transfer in channel flow with dimpled surfaces: Application to heat sinks in microelectronic cooling. J Electron Packag Trans ASME 2007;129:157–66. https://doi.org/10.1115/1.2721087.

[45] Wei XJ, Joshi YK, Ligrani PM. Numerical simulation of flow and heat transfer inside a micro-channel with one dimpled surface. ASME Int Mech Eng Congr Expo Proc 2002;7:149–56. https://doi.org/10.1115/IMECE2002-33725.

[46] Chang SW, Jan YJ, Chang SF. Heat transfer of impinging jet-array over convex-dimpled surface. Int J Heat Mass Transf 2006;49:3045–59. https://doi.org/10.1016/j.ijheatmasstransfer.2006.02.030.

[47] Xie G, Liu J, Ligrani PM, Zhang W. Numerical predictions of heat transfer and flow structure in a square cross-section channel with various non-spherical indentation dimples. Numer Heat Transf Part A Appl 2013;64:187–215. https://doi.org/10.1080/10407782.2013.779485.

[48] Xie G, Sundn B, Zhang W. Comparisons of pins/dimples/protrusions cooling concepts for a turbine blade tip-wall at high Reynolds numbers. J Heat Transfer 2011;133:1–9. https://doi.org/10.1115/1.4003558.

[49] Elyyan MA, Rozati A, Tafti DK. Investigation of dimpled fins for heat transfer enhancement in compact heat exchangers. Int J Heat Mass Transf 2008;51:2950–66. https://doi.org/10.1016/j.ijheatmasstransfer.2007.09.013.

[50] Wang S, Yan H, Luo L, Du W, Sundén B, Zhang X. Heat transfer characteristics of a dimpled/protrusioned pin fin wedge duct with different converging

angles for turbine blades. Numer Heat Transf Part A Appl 2019;76:369–92. https://doi.org/10.1080/1040 7782.2019.1630235.

[51] Sparrow EM, Gorman JM, Friend KS, Abraham JP. Flow regime determination for finned heat exchanger surfaces with dimples/protrusions. Numer Heat Transf Part A Appl 2013;63:245–56. https://doi.org/10.1080/10407782.2013.730450.

[52] Xie G, Sundén B. Numerical predictions of augmented heat transfer of an internal blade tip-wall by hemispherical dimples. Int J Heat Mass Transf 2010;53:5639–50. https://doi.org/10.1016/j.ijheatmasstransfer.2010.08.019.

[53] Kim HM, Moon MA, Kim KY. Shape optimization of inclined elliptic dimples in a cooling channel. J Thermophys Heat Transf 2011;25:472–6. https://doi.org/10.2514/1.T3674.

[54] Won SY, Ligrani PM. Flow characteristics along and above dimpled surfaces with three different dimple depths within a channel. J Mech Sci Technol 2007;21:1901–9. https://doi.org/10.1007/BF03177447.

[55] Karim MA, Hawlader MNA. Performance investigation of flat plate, v-corrugated and finned air collectors. Energy 2006;31:452–70. https://doi.org/10.1016/j.energy.2005.03.007.

[56] Choudhury C, Garg HP. Design analysis of corrugated and flat plate solar air heaters. Renew Energy 1991;1:595–607. https://doi.org/10.1016/0960-1481(91)90003-8.

[57] Abdul -Malik Ebrahim Momin, J.S Saini S. S. Heat transfer and friction in solar air heater duct with V-Shaped rib roughness on an absorber plate. Int J Heat Mass Transf 2002;45:3383–96.

[58] Karim MA, Hawlader MNA. Development of solar air collectors for drying applications. Energy Convers Manag 2004;45:329–44. https://doi.org/10.1016/S0196-8904(03)00158-4.

[59] A.E KABEEL KM. Shape optimization for absorber plates of solar air collectors. Renew Energy 1998;13:121–31.

[60] Kabeel AE, Khalil A, Shalaby SM, Zayed ME. Investigation of the Thermal Performances of Flat, Finned, and v-Corrugated Plate Solar Air Heaters. J Sol Energy Eng 2016;138:051004. https://doi.org/10.1115/1.4034027.

[61] HACHEMI A, Performance T, Of E, Plate BYAFA, Fins WR. Air Heaters , By a Fan-Blown Absorber Plate. Int Energy J 1995;19:567–77.

[62] Akpinar EK, Koçyiğit F. Experimental investigation of thermal performance of solar air heater having different obstacles on absorber plates. Int Commun Heat Mass Transf 2010;37:416–21. https://doi.org/10.1016/j.icheatmasstransfer.2009.11.007.

[63] Ong KS. Thermal performance of solar air heaters- experimental correlation. Sol Energy 1995;55:209–20.

[64] Yeh H, Lin T. Efficiency improvement of flat-plate solar air heaters. Energy 1996;21:435–43.

[65] Bhushan B, Singh R. A review on methodology of artificial roughness used in duct of solar air heaters. Energy 2010;35:202–12. https://doi.org/10.1016/j.energy.2009.09.010.

[66] Leon O, De Mey G, Dick E, Vierendeels J. Comparison between the standard and staggered layout for cooling fins in forced convection cooling. J Electron Packag Trans ASME 2003;125:442–6. https://doi.org/10.1115/1.1602709.

[67] Fakoor Pakdaman M, Lashkari A, Basirat Tabrizi H, Hosseini R. Performance evaluation of a natural-convection solar air-heater with a rectangular-finned absorber plate. Energy Convers Manag 2011;52:1215–25. https://doi.org/10.1016/j.enconman.2010.09.017.

[68] Zetty Akhtar AM, Rahman MM, Kadirgama K, Rahman S, Maleque MA. Thermal Conductivity and Viscosity of TiO2/MWCNTs (doped 10wt% graphene) - Ethylene Glycol Based Nanofluids for Different Ratio of Nanoparticle. J Adv Res Fluid Mech Therm Sci 2020;72:32–46. https://doi.org/10.37934/arfmts.72.1.3246.

[69] Hussein AK, Li D, Kolsi L, Kata S, Sahoo B. A Review of Nano Fluid Role to Improve the Performance of the Heat Pipe Solar Collectors. Energy Procedia 2017;109:417–24. https://doi.org/10.1016/j.egypro.2017.03. 044.